Journal of Hydrology 411 (2011) 219–237

Contents lists available at SciVerse ScienceDirect

Journal of Hydrology

journal homepage: www.elsevier.com/locate/jhydrol

The Surface Urban Energy and Water Balance Scheme (SUEWS): Evaluation in Los Angeles and Vancouver

L. Järvi [a,b], C.S.B. Grimmond [a,*], A. Christen [c]

[a] King's College London, Department of Geography, The Strand, WC2R 2LS London, UK
[b] Department of Physics, P.O Box 48, University of Helsinki, Finland
[c] University of British Columbia, Department of Geography, 1984 West Mall, Vancouver, B.C., Canada

ARTICLE INFO

Article history:
Received 25 January 2011
Received in revised form 20 September 2011
Accepted 2 October 2011
Available online 8 October 2011
This manuscript was handled by Konstantine P. Georgakakos, Editor-in-Chief, with the assistance of Ashish Sharma, Associate Editor

Keywords:
Urban water balance
Surface conductance
Evaporation
Urban energy balance
Vancouver
Los Angeles

SUMMARY

An urban energy and water balance model is presented which uses a small number of commonly measured meteorological variables and information about the surface cover. Rates of evaporation-interception for a single layer with multiple surface types (paved, buildings, coniferous trees and/or shrubs, deciduous trees and/or shrubs, irrigated grass, non-irrigated grass and water) are calculated. Below each surface type, except water, there is a single soil layer. At each time step the moisture state of each surface is calculated. Horizontal water movements at the surface and in the soil are incorporated. Particular attention is given to the surface conductance used to model evaporation and its parameters. The model is tested against direct flux measurements carried out over a number of years in Vancouver, Canada and Los Angeles, USA. At all measurement sites the model is able to simulate the net all-wave radiation and turbulent sensible and latent heat well (RMSE = 25–47 W m^{-2}, 30–64 and 20–56 W m^{-2}, respectively). The model reproduces the diurnal cycle of the turbulent fluxes but typically underestimates latent heat flux and overestimates sensible heat flux in the day time. The model tracks measured surface wetness and simulates the variations in soil moisture content. It is able to respond correctly to short-term events as well as annual changes. The largest uncertainty relates to the determination of surface conductance. The model has the potential be used for multiple applications; for example, to predict effects of regulation on urban water use, landscaping and planning scenarios, or to assess climate mitigation strategies.
© 2011 Elsevier B.V. All rights reserved.

1. Introduction

In urban areas the water and energy exchanges are altered by land cover changes and peoples' behavior. Compared to naturally vegetated areas, urban land cover changes result in increases in surface runoff, reduction in evaporation and increased sensible heat emissions to the urban boundary layer (Mitchell et al., 2003, 2008; Xiao et al., 2007). These have implications for flooding (Schiff et al., 2007), human comfort (McMichael et al., 2008), mixing of the boundary layer and pollutant dispersion. Despite the importance of urban areas, given half the world's population lives in cities, energy and water balance fluxes are rarely measured. This information is important for decision and policy makers operating at a range of spatial scales (properties, blocks, neighborhoods, cities) relating to the provision of water or imposing water restrictions, mitigating or responding to extreme conditions for human comfort, and air pollution prediction and exposure alerts. Of interest are both high magnitude – low frequency events (e.g. flooding) and low magnitude-high frequency events (e.g. air pollution exposure). These require continuous knowledge of the state of the surface and the atmosphere to assess risks and vulnerabilities for urban residents.

For urban areas the water balance of the external environment can be written (Grimmond et al., 1986):

$$P + I_e + F = E + R + \Delta S \quad [\text{mm h}^{-1}] \tag{1}$$

where P is precipitation, I_e is the external piped water supply, F is the anthropogenic water emission (e.g. combustion, air conditioning, human emissions from breathing), E is the evaporation (which includes transpiration), R is the runoff, and ΔS the net change in water storage (e.g. changes in soil moisture, detention ponds) within the study area. When the complete urban environment is considered the piped water used internally within buildings is included. Through evaporation the water balance is linked to the energy balance which in urban areas is written (Oke, 1987):

$$Q^* + Q_F = Q_E + Q_H + \Delta Q_S \quad [\text{W m}^{-2}] \tag{2}$$

where Q^* is the net all-wave radiation, Q_F is the anthropogenic heat emission, Q_E is the latent heat flux ($Q_E = L_v E$; L_v is the latent heat of vaporization), Q_H is the turbulent sensible heat flux, and ΔQ_S is the net storage heat flux which includes soil heat flux and also the heating and cooling of the complete urban fabric. Although advection

* Corresponding author. Tel.: +44 207 848 2275; fax: +44 207 848 2287.
E-mail address: sue.grimmond@kcl.ac.uk (C.S.B. Grimmond).

0022-1694/$ - see front matter © 2011 Elsevier B.V. All rights reserved.
doi:10.1016/j.jhydrol.2011.10.001

exists it is dealt with either through larger scale models in which land surface models are embedded or at the micro-scale advection is included within the parameterizations of the individual terms.

Many of the earliest studies of the urban water balance used the available data to estimate the terms of the water balance, but often the methods of determination were not explicitly stated (Aston, 1977; Bell, 1972; Campbell, 1982; Lindh, 1978). One of the first models, L'vovich and Chernogayeva (1977) used observed precipitation data with modeled runoff to determine the evaporation by residual. Although numerous models have been developed for urban runoff they do not account for the complete urban water balance (e.g. Berthier et al., 2004). Distributed hydrological models have been modified to account for urban areas but to date the emphasis has been on runoff (e.g. Cuo et al., 2008).

Some urban water balance models have been developed at the individual property scale with attention to conserving irrigation water and reducing runoff (Mitchell et al., 2001; Xiao et al., 2007). Particularly in arid regions, calculation of the amount of water used for irrigation is of key interest. To do this potential evaporation is calculated, which may be modified with crop coefficients (Xiao et al., 2007).

Actual evapotranspiration (or latent heat flux) can be measured by eddy covariance techniques at the neighborhood or local scale (10^2–10^4 m). Grimmond et al. (1986), the first to present a water balance model for urban areas with actual evaporation rates at this scale, accounted for the surface and soil at a daily time step. Grimmond and Oke (1991), using an evaporation-interception approach, calculated hourly fluxes. However, their model used a large number of observed variables, such as soil moisture, irrigation rates, and net all wave radiation. Lemonsu et al.'s (2007) combined Town Energy Balance and soil-vegetation-atmosphere-transfer scheme (TEB-ISBA) examined both urban runoff and the energy balance to determine infiltration of water through roads.

Not all urban energy balance models simulate latent heat flux, and they rarely account for irrigation and runoff processes. The 'PILPS-urban' international comparison of urban energy balance models (Grimmond et al., 2010, 2011) concluded that the inclusion of the latent heat flux was important, even in areas with little vegetation and that overall it was the most poorly modeled flux. The model comparison documented a vast range in model performance and concluded there is no individual model that had the best performance for all fluxes. Application of several models, to provide an ensemble, resulted in the lowest modeled error (Grimmond et al., 2011).

Thus while there is growing interest in urban energy and water exchange processes there remains a need for a model that can simulate both energy and water fluxes for extended periods of time (e.g. multiple years) that requires only limited input data that can be acquired from standard meteorological stations or a meso-scale model. This work attempts to fill that gap. Here previously published models are combined with new parameterizations to form the **S**urface **U**rban **E**nergy and **W**ater **B**alance **S**cheme (hereafter SUEWS), which calculates energy and water balances at the neighborhood scale (Fig. 1). The foundations of SUEWS, the urban evaporation-interception scheme of Grimmond and Oke (1991) and the urban water balance model of Grimmond et al. (1986), are combined with additional modules to reduce the number of required input variables (Table 1) and to include more fully the energy and water exchange processes. The goal is to provide a widely applicable model for researchers and urban planners which could be embedded into larger scale models or operate on a stand-alone basis. Unlike most urban land surface models (Grimmond et al., 2009, 2011), the surface resistance scheme is parameterized explicitly for urban areas rather than using schemes originally designed for non-urban areas and takes an integrated approach to the inclusion of urban vegetation.

2. The model

This paper describes the SUEWS scheme, with particular attention to surface conductance used in the Penman–Monteith equation (Monteith, 1965; Penman, 1948). Several methods have been developed to model surface conductance (Irmak and Mutiibwa, 2010), given it is difficult to measure yet is very important for the exchange of water between the surface and the atmosphere. Here the Jarvis (1976) approach is used to obtain general coefficients for urban environments.

To simulate urban water and energy balances, Eqs. (1) and (2), SUEWS uses several sub-models (Fig. 1a) which are designed to minimize the number of input variables required (Table 1) (see Appendix A for notation). The model takes both the surface and the soil below into account. Both are treated as single-layer moisture stores. The surface stores allow for the full array of surface types observed in urban environments (Fig. 1b) – paved areas, roofs, coniferous trees and shrubs, deciduous trees and shrubs, irrigated grass, non-irrigated grass and water – to be considered. Each surface type, except water, has a soil store below. When saturation of the soil occurs, the excess water is either prevented from entering the soil creating surface runoff and/or passes out of the bottom of the modeled soil layer, this is termed deep soil runoff.

The fundamental spatial scale of the model is the neighborhood or local scale. This makes it suitable for inclusion as a tile within a meso-scale meteorological model or unit within a larger hydrological model. The fundamental grid area and shape are not fixed. The model can be run for an individual area or grid cell representative of a neighborhood or multiple hydrological linked (or unlinked) grids which make up catchments or watersheds. However, for comparison with directly measured turbulent fluxes these need to have similar dimensions to a flux source area (10^2–10^4 m length scale). Besides commonly measured meteorological variables (wind speed, relative humidity, air temperature, pressure, precipitation, shortwave irradiance) the model requires information for each model grid, including: the plan area fraction of each surface type, number of inhabitants, fraction of irrigated area using automatic sprinklers; and internal hydrological connectivity (for example, based on elevation differences or pervious/impervious linkages or by piped network connectivity) (Appendix A).

The basic time step for SUEWS is 5 min to hourly, results are aggregated into daily, monthly and annual time periods. SUEWS can be run for periods of a day (or less) to multiple years with changing surface characteristics and meteorological forcing. Thus, the development of an area through time can be taken into account.

2.1. Available energy

The magnitude of sensible and latent heat fluxes are dependent on the available energy, which is determined from the net all-wave radiation (Q^*), net storage heat flux (ΔQ_S) and anthropogenic heat flux (Q_F). These are typically calculated with a 1 h time step.

For SUEWS, Q^* is calculated using the net all-wave radiation parameterization scheme (NARP) (Loridan et al., 2011; Offerle et al., 2003). This allows Q^* to be calculated using incoming shortwave radiation ($K\downarrow$), relative humidity (RH) and air temperature (T). Instead of the latter two variables, incoming long-wave radiation or cloud cover can be used if available; both improve the Q^* parameterization (Loridan et al., 2011). The effect of snow on the surface albedo and Q^* can be taken into account in the input data file by defining the fraction of surface covered by snow. ΔQ_S is calculated using the Objective Hysteresis Model (OHM; Grimmond and Oke, 1999a, 2002) which is able to capture the characteristic

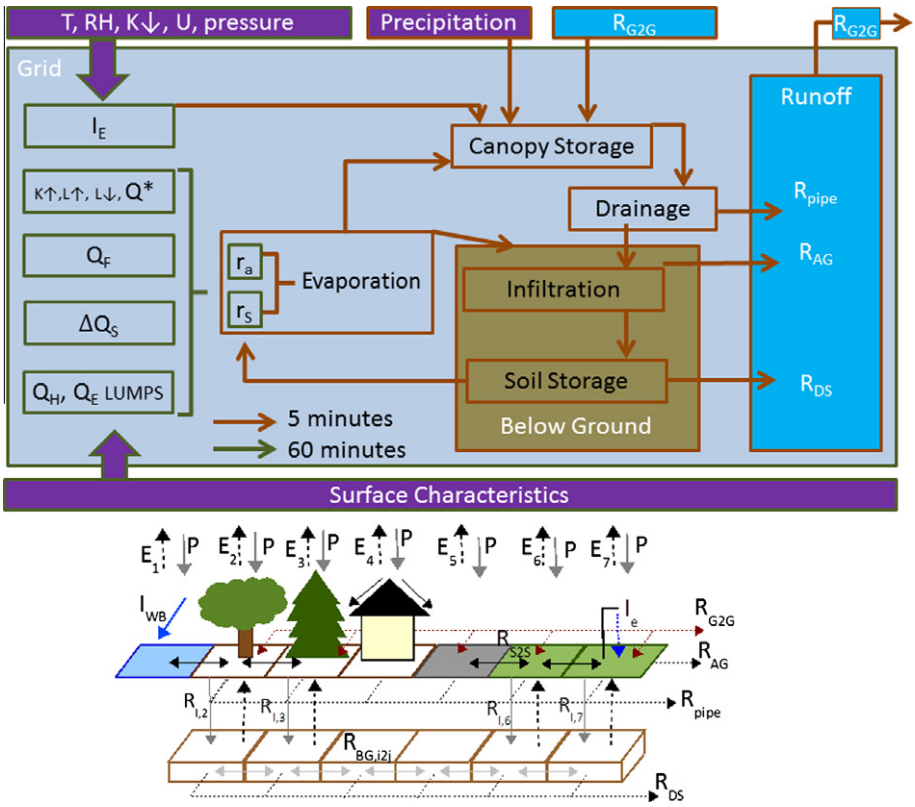

Fig. 1. SUEWS (upper) order of calculations within a grid cell and between grids; (lower) conceptual diagram of the seven parallel surface types (i) with the horizontal and vertical flows of water (see text for details) within a grid cell and between grid cells. E is the evapotranspiration, P the precipitation, I_e the external irrigation, R runoff (see text and Appendix A for details of notation).

magnitude and diurnal hysteresis of the storage heat flux in cities (Offerle et al., 2005; Roberts et al., 2006).

To calculate Q_F, we modify the Sailor and Vasireddy (2006) approach developed for the calculation of residential electricity usage. This approach employs cooling and heating degree days (CDD and HDD, respectively) in order to take into account energy used for heating in cold temperatures and increased air conditioning in warm temperatures. The daily anthropogenic heat flux (W m^{-2}) per population density (p, units: capita ha^{-1}) is calculated for weekdays (wd) and weekends (we)

$$Q_{F_{p,\{wd,we\}}} = a_{0\{wd,we\}} + a_{1\{wd,we\}}CDD + a_{2\{wd,we\}}HDD \quad (3)$$

where $a_{0,\{wd,we\}}$ is the base value of Q_F which is the integrated heat flux per p from all sources relative to a base human comfort temperature (e.g. 18.2 °C, Sailor and Vasireddy, 2006) for wd and we. The relation for a study area between CDD ($a_{1,\{wd,we\}}$) and HDD ($a_{2,\{wd,we\}}$) needs to be specified. The daily Q_F is partitioned using user-definable diurnal profiles for we and wd (Table 3). Alternatively, SUEWS can use Q_F as an input data set if it is available; the Large scale Urban Consumption of energy model (LUCY) provides one such option (Allen et al., 2010). LUCY simulates all components of anthropogenic heat flux from the global to individual city scale hourly at 2.5 × 2.5 arc-minute resolution.

2.2. Leaf area index (LAI)

To allow for changes in the growing season between years, a dynamic response of leaf area index (LAI) to growing degree days (GDD) and senescence degree days (SDD) (to capture the effect of temperature on the initiation of leaf-off in the autumn) has been developed. LAI is used in the calculation of surface conductance (Section 2.4.2) and it controls seasonal behavior of the vegetation porosity for roughness length calculations, surface albedo and water storage capacity of deciduous trees. The leaf-on period is determined by GDD and the start of the leaf-off period by the SDD.

The daily $LAI_{d,i}$ for each vegetation type (i) is:

$$\begin{cases} LAI_{d,i} = LAI_{d-1,i}^{0.03} GDD \cdot 5 \cdot 10^{-4} + LAI_{d-1,i}, & T_{BaseSDD} < T_d < T_{BaseGDD} \\ LAI_{d,i} = LAI_{d-1,i}^{0.03} SDD \cdot 5 \cdot 10^{-4} + LAI_{d-1,i}, & T_{BaseGDD} < T_d < T_{BaseSDD} \end{cases} \quad (4)$$

where $LAI_{d-1,i}$ is LAI of vegetation surface type i from the previous day, T_d is the mean daily temperature and $T_{BaseGDD}$ and $T_{BaseSDD}$ are the base temperatures for initiating the periods of leaf-on and leaf-off, respectively. The user-defined minimum LAI should always be larger than zero for each vegetation type.

2.3. External water use I_e

I_e is an important additional input to the urban water balance and can easily exceed the volume of water from precipitation (Grimmond and Oke, 1986; Mitchell et al., 2001, 2003). For some cities and regions, it is the only input of water for large parts of the year. If I_e data are not available a simple hourly model can be used. The probable daily water used (mm d^{-1}) is calculated from T_d and time since rain (t_r, d) according to:

$$I_e = f_{Irrgrass}[f_{aut}(b_{0,a} + b_{1,a}T_d + b_{2,a}t_r) + (1 - f_{aut})(b_{0,m} + b_{1,m}T_d + b_{2,m}t_r)] \quad (5)$$

where f_{aut} is the fraction of irrigated area $f_{Irrgrass}$ using automatic irrigation, $b_{0,a}$–$b_{2,a}$ and $b_{0,m}$–$b_{2,m}$ are site specific coefficients for automatic and manual irrigation, respectively. Automatic and manual irrigation are considered separately as they tend to differ in terms of the time of day at which they occur and their response

Table 1
Required (a) meteorological input and (b) output variables of the model. See text for further comments about the use of additional input variables (if available). See Appendix A for the parameters required. The spatial scale the data are representative of are: local scale or the whole grid (Loc) and individual surface types within a gird (T). Larger areas can be determined from the individual grids.

Variable	Units	Spatial scale
(a) Input		
Mean wind speed (u)	m s^{-1}	Loc
Relative humidity (RH)	%	Loc
Air temperature (T)	°C	Loc
Station air pressure	kPa	Loc
Precipitation (P)	mm h^{-1}	Loc
Incoming short wave radiation ($K\downarrow$)	W m^{-2}	Loc
(b) Output		
Net all-wave radiation (Q^*)	W m^{-2}	Loc, T
Radiation components: $K\uparrow$, $L\uparrow$, $L\downarrow$	W m^{-2}	Loc, T
Surface temperature	°C	Loc, T
Sensible heat flux – LUMPS (Q_H)	W m^{-2}	Loc
Latent heat flux – LUMPS (Q_E)	W m^{-2}	Loc
Storage heat flux (ΔQ_S)	W m^{-2}	Loc
Anthropogenic heat flux (Q_F)	W m^{-2}	Loc
Sensible heat flux – SUEWS (Q_H)	W m^{-2}	Loc
Latent heat flux – SUEWS (Q_E)	W m^{-2}	Loc
Evapotranspiration (E)	mm h^{-1}	Loc
External water use (I_e)	mm h^{-1}	Loc
Drainage (D)	mm h^{-1}	Loc, T
State of the surface storages (C_i)	mm	Loc, T
Aerodynamic resistance (r_a)	s m^{-1}	Loc
Surface resistance (r_s)	s m^{-1}	Loc
Friction velocity (u_*)	m s^{-1}	Loc
Obukhov length (L)	m	Loc
Soil moisture deficit ($\Delta\theta$)	mm	Loc, T
Leaf area index (LAI)	m^2 m^{-2}	Loc
Runoff ($R = R_{Pipe} + R_{AG}$)	mm	Loc, T
Runoff to pipes (R_{pipe})	mm	Loc
Above ground runoff (R_{AG})	mm	Loc
Deep soil runoff (R_{DS})	mm	Loc, T

to local weather conditions. The diurnal cycle is obtained using water profiles applied to the daily external water use (Table 3). Given that water use restrictions are widely used in different cities (e.g. Gober et al., 2010; MacDonald et al., 2010), SUEWS allows water profiles to be defined so that the impact of different water restriction schedules can be evaluated (importantly the model also provides a framework to evaluate such regimes). The start and end times ($I_{e,start}$ and $I_{e,end}$, respectively) of the external irrigation season have to be specified.

2.4. Turbulent heat fluxes

Evaporation from each surface is calculated with the Penman–Monteith equation (Monteith, 1965; Penman, 1948) modified for urban areas (Grimmond and Oke, 1991):

$$Q_E = \frac{s(Q^* + Q_F - \Delta Q_S) + c_p \rho V / r_a}{s + \gamma(1 + r_s/r_a)} \quad (6)$$

This is applicable to dry surfaces. When the surface is completely wet the surface resistance r_s is set to zero. To link the two surface stages (dry and wet), r_s is replaced with a redefined surface resistance r_{ss} (Shuttleworth, 1978):

$$r_{ss} = \left[\frac{W}{r_b(s/\gamma + 1)} + \frac{(1 - W)}{r_s + r_b(s/\gamma + 1)}\right]^{-1} - r_b(s/\gamma + 1) \quad (7)$$

where W is a function of the amount of water on the canopy of the individual surface surfaces (C_i) relative to the canopy surface water storage capacity (S_i):

$$W = 1 \qquad C_i \geqslant S_i$$
$$W = (K - 1)/(K - S_i/C_i) \qquad C_i < S_i$$

and K relates to the aerodynamic (r_a) and surface (r_s) resistances:

$$K = \frac{(r_s/r_a)/(r_a - r_b)}{r_s + r_b(s/\gamma + 1)}$$

where r_b is the boundary layer resistance (Shuttleworth, 1983):

$$r_b = 1.1u_*^{-1} + 5.6u_*^{\frac{1}{3}}$$

Q_E depends on the surface wetness state and therefore it is calculated with 5 min time step. Sensible heat flux is calculated as a residual from the hourly available energy minus the hourly latent heat flux.

2.4.1. Aerodynamic resistance r_a

The aerodynamic resistance is calculated using the logarithmic wind profile for each hour:

$$r_a = \frac{[ln(\frac{z_m - z_d}{z_{0m}}) - \psi_m][ln(\frac{z_m + z_d}{z_{0v}}) - \psi_v]}{k^2 u}, \quad (8)$$

where z_m is the height of the measured horizontal wind speed u, z_d is the zero plane displacement height, z_{0m} is the roughness length for momentum, z_{0v} is the roughness length for heat and water vapor, k is the von Karman constant (0.4), and ψ_m and ψ_v are the stability functions for momentum and water vapor, respectively The stability functions for unstable conditions for momentum are (van Ulden and Holtslag, 1985):

$$\psi_m = 2\ln\left(\frac{1 + X}{2}\right) + ln\left(\frac{1 + X^2}{2}\right) - 2tan^{-1}(X) + \frac{\pi}{2} \quad (9)$$

where $X = (1 - 15.2\zeta)^{0.25}$ (Högström, 1988) and $\zeta = (z_m - z_d)/L$ and for heat and water vapor (van Ulden and Holtslag, 1985):

$$\psi_v = 2ln\left(\frac{1 + Y^2}{2}\right) \quad (10)$$

where $Y = 0.95(1 - 15.2\zeta)^{0.5}$ (Högström, 1988). The function for stable condition for momentum (van Ulden and Holtslag, 1985):

$$\psi_m = -17(1 - \exp(-0.29\zeta)) \quad (11)$$

and for heat and water vapor (Högström, 1988):

$$\psi_v = -4.5\zeta \quad (12)$$

The initial calculation of the stability functions uses Q_H calculated at each time step by the local-scale urban parameterization scheme (LUMPS) (Grimmond and Oke, 2002).

The evaluation of z_{0m} and z_d schemes by Grimmond and Oke (1999b) was driven by the sensitivity of the r_a to the values used. In SUEWS, z_{0m} and z_d may be specified (static or dynamic) or calculated using Macdonald et al. (1998) or rule of thumb (Grimmond and Oke, 1999b). If these are calculated in SUEWS, the mean height of roughness elements is determined as a weighted average from the mean height of buildings and trees, and takes into account that the trees are not bluff bodies. The porosity of trees is set to vary with LAI of the deciduous trees (Grimmond and Oke, 1999b). When evaluating the model against measurements the changing observational footprint can be accounted for if the user provides values for each interval (dynamic).

Assuming the roughness length for heat and moisture are the same, then z_{0v} is typically calculated from z_{0m}. Recently, parameterizations for urban areas have been developed (Kanda et al., 2007; Voogt and Grimmond, 2000) of the general form (Brutsaert, 1982):

Table 2
(a) Model parameter values by surface type and (b) general model run options (see Appendix A for notation and units, and text for relevant equations where the parameters are used). Initial state for soil stores in Vancouver (VCR) and Los Angeles (LA) are set to different values because of the different hydro-meteorological conditions.

(a)	Units	Building	Pavement	Conif. Trees	Decid. trees	Irrigated grass	Unirrigated grass	Water
S_i	mm	0.25[a]	0.48[b]	1.3[c]	0.3–0.8[c]	1.9[c]	1.9[c]	0
$S_{soil,i}$	mm	150[d]	150[d]	150[d]	150[d]	150[d]	150[d]	–
$D_{0,i}$	mm	10[e]	10[e]	0.013[e]	0.013[e]	10[e]	0.013[e]	–
b	–	3[d]	3[d]	1.71[d]	1.71[d]	0.013[d]	1.71[d]	–
C_i	mm	0	0	0	0	0	0	0
$C_{soil,i}$	mm VCR	150[d]	150[d]	150[d]	150[d]	150[d]	150[d]	–
	LA	130	130	130	130	130	145	
α_i	–	0.15[f]	0.12[f]	0.10[f]	0.18[f]	0.21[f]	0.21[f]	0.10[f]
ε_i	–	0.95[f]	0.91[f]	0.98[f]	0.98[f]	0.93[f]	0.93[f]	0.95[f]
$g_{i,max}$	mm s^{-1}	–	–	7.4[c]	11.7[c]	40	33.1[c]	–
(b) Input	*Value*	*Input*	*Value*	*Input*	*Value*	*Input*	*Value*	
α_{snow}	0.5	$b_{2,m}$	1.10	K_s	0.0005[g]	S_1	0.45	
ε_{snow}	0.99	G_1	16.48	$LAI_{max,con}$	5.1[c]	S_2	15	
ρ_{soil}	-	G_2	566.1	$LAI_{max,dec}$	5.5[c]	S_{Pipe}	100	
$a_{0,\{wd,we\}}$	0.308	G_3	0.216	$LAI_{max,grass}$	5.9[c]	SDD	−450	
$a_{1,\{wd,we\}}$	$9.86{\cdot}10^3$	G_4	3.36	$LAI_{min,con}$	4	$T_{BaseGDD}$	5	
$a_{2,\{wd,we\}}$	0.0102	G_5	11.07	$LAI_{min,dec}$	1	$T_{BaseSDD}$	11	
$b_{0,a}$	−84.54	G_6	0.018	$LAI_{min,grass}$	1.6[i]	T_{BaseQF}	18.2[h]	
$b_{1,a}$	9.96	GDD	300	$r_{s,max}$	9999.0	T_H	40	
$b_{2,a}$	3.67	I_W	0.0	res_{cap}	10[j]	T_L	0	
$b_{0,m}$	−25.36	$K{\downarrow}_m$	1200	res_{drain}	0.25[j]	T_{step}	300	
$b_{1,m}$	3.00			R_C	1.0[j]			

[a] Falk and Niemczynowicz (1978).
[b] Davies and Hollis (1981).
[c] Breuer et al. (2003).
[d] Grimmond et al. (1986).
[e] Grimmond and Oke (1991).
[f] Oke (1987).
[g] Berthier et al. (2006).
[h] Sailor and Vasireddy (2006).
[i] Grimmond (1988).
[j] Loridan et al. (2010).

$$z_{0v} = z_{om}\exp\left(2.0 - a\frac{z_{0m}u_*}{v}\right) \tag{13}$$

where a is an empirical constant depending on the surface cover and $v = 1.46 \cdot 10^{-5}\ m^2\ s^{-1}$ is the molecular viscosity of air. For unvegetated urban surfaces, Kanda et al. (2007) proposed $a = 1.29$. We use Kawai et al. (2009):

$$a = 1.2 - 0.9f_v^{0.29} \tag{14}$$

where a depends on the fraction of vegetation cover (f_v).

2.4.2. Surface resistance r_s

Evaporation is highly sensitive to r_s (or its inverse surface conductance g_s) thus defining it appropriately is important. Here a single integrated conductance for the whole surface is calculated using a modified version of the physically based model of Jarvis (1976) and Grimmond and Oke (1991):

$$r_s^{-1} = g_S = G_1\sum_{i=3}^{6}\left(f_i g_{i,max}\frac{LAI_{d,i}}{L_{m,i}}\right)g(K{\downarrow})g(\Delta q)g(T)g(\Delta\theta) \tag{15}$$

This allows g_s to respond by vegetation type (i) to $LAI_{d,i}$ relative to its maximum ($L_{m,i}$) for its fraction of cover (f_i) and maximum conductance values ($g_{i,max}$), and the environmental variables of incoming shortwave radiation ($K{\downarrow}$, W m^{-2}):

$$g(K{\downarrow}) = \frac{K{\downarrow}/(G_2 + K{\downarrow})}{K{\downarrow}_m/(G_2 + K{\downarrow}_m)}$$

specific humidity deficit (Δq, g kg^{-1}):

$$g(\Delta q) = \begin{cases} 1 - G_3\Delta q, \Delta q < G_4 \\ 1 - G_3G_4, \Delta q \geqslant G_4 \end{cases}$$

air temperature (T, °C):

$$g(T) = \frac{(T - T_L)(T_H - T)^{T_c}}{(G_5 - T_L)(T_H - G_5)^{T_c}}$$

where $T_c = (T_H - G_5)/(G_5 - T_L)$, and soil moisture deficit ($\Delta\theta$, mm):

$$g(\Delta\theta) = 1 - \exp\{G_6(\Delta\theta - (S_1/G_6) + S_2)\}$$

where S_1 and S_2 are parameters related to the maximum $\Delta\theta$.

To obtain the parameters G_1–G_6 (Section 4.2) observations of Q_H and Q_E (Section 3) are used to determine 'measured' values of r_s from:

$$r_s = \left(\frac{s\beta}{\gamma} - 1\right)r_a + \frac{c_p\rho V}{\gamma Q_E} \tag{16}$$

2.5. Interception state of the canopy (C_i), infiltration (R_I), and runoff (R)

For the calculation of flowing water the model has a 5 min time step to allow rapid response to rain or irrigation events (Grimmond and Oke, 1991). The equations are given for the current time step unless otherwise indicated. The surface wetness state of ith surface (C_i) determines the approach taken for calculating evaporation from Eq. (6). At each time step a running water balance of each surface i (Rutter et al., 1971) is calculated, which has the form (Grimmond and Oke, 1991):

$$C_i = C_{i,t-1} + (P_i + I_{e,i} + R_{G2G,i} + R_{S2S,i}) - (D_i + E_i) \quad (\text{in mm } (5\text{ min})^{-1}) \tag{17a}$$

The surface can become wet from precipitation (P_i), irrigation ($I_{e,i}$) or from runoff from water flowing above ground from a neighboring grid ($R_{G2G,i}$) and/or from within the grid from hydrologically connected surfaces ($R_{S2S,i}$). The amount of water received by this

Table 3
Diurnal profiles of (a) Q_F for a residential area in Vs87 for weekdays (*wd*) and weekends (*we*). These are applied to the mean daily flux (3). (b) External water use. The model allows for daily water use profiles (Prof) to be specified (when actual water use data are not supplied) as a fraction of the daily total (5) for a particular time period. A constant amount of water use is assumed for each hour with a delineated period.

h	(a) Q_F		(b) Fraction I_e		
	wd	*we*	Prof 1 Vancouver[a]	Prof 2 Arcadia[b]	Prof 3 San Gabriel[b]
0	0.57	0.65			
1	0.45	0.49			
2	0.43	0.46			
3	0.40	0.47	0.15	0.40	0.35
4	0.40	0.47			
5	0.45	0.53			
6	0.71	0.70			
7	1.20	1.13			
8	1.44	1.37			
9	1.29	1.37			
10	1.28	1.30			
11	1.31	1.37	0.35	0.40	0.19
12	1.30	1.33			
13	1.32	1.30			
14	1.35	1.27			
15	1.44	1.36			
16	1.51	1.44			
17	1.41	1.30	0.50	0.20	0.46
18	1.14	1.10			
19	0.99	0.98			
20	0.86	0.84			
21	0.85	0.90			
22	0.80	0.87			
23	0.70	0.74			

[a] Based on Vs87 data.
[b] Grimmond et al. (1996).

inter-surface transfer within a grid is specified by the user based on hydrological connectivity with the impacts of topographic differences taken into account. For the water surface no drainage occurs. However, when grid to grid flow occurs there is a stream/river, whereas when there is no flow there is a detention pond. If the water body receives external water it may be necessary to account for this (I_{WB}) through input by the user.

$$C_{water} = C_{water,t-1} + (P_i + I_{WB} \pm R_{G2G,water} + R_{S2S,water}) - E_i) \quad (17b)$$

Drainage (D_i), the rate at which a surface store drains, depends on the surface type (i) and the water status of the surface (or store) from the previous time step ($C_{i,t-1}$); for unirrigated vegetation (Halldin et al., 1979) this is:

$$D_i = D_{0,i} exp(bC_{i,t-1} - 1) \quad (18)$$

and for paved surface, roofs and irrigated vegetation (Falk and Niemczynowicz, 1978):

$$D_i = D_{0,i}(C_{i,t-1})^b. \quad (19)$$

The values for the maximum drainage rates ($D_{0,i}$) and coefficients (b) are taken from the literature (Table 2).

From both impervious and pervious surfaces part of drainage water can flow to hydrologically connected surfaces ($D_{S2S,i}$); for example, allowing water to drain from the roof to an impervious or vegetated area (see also $R_{S2S,i}$). From impervious surfaces, the drainage not flowing to neighboring surfaces goes to the pipe network (C_{pipe}) as runoff ($R_{pipe,i}$):

$$C_{pipe,t} = C_{pipe,t-1} + \sum_{i=1}^{2} R_{pipe,i} \quad (20)$$

If the pipe capacity (S_{pipe}) is exceeded flooding above ground occurs as the water is added to above ground runoff ($R_{AG,imp}$):

$$R_{AG,imp} = (C_{pipe} - S_{pipe}) \quad (21)$$

Currently, for impervious surfaces water cannot infiltrate to the soil directly (for example, cracks in the pavement are assumed not to exist).

From pervious surfaces, part of the drainage infiltrates ($R_{I,j}$) into the underlying soil increasing the amount of water of each subsurface i ($C_{soil,i}$). It is assumed that the soil infiltration rate is larger than drainage (Grimmond and Oke, 1986) if rainfall intensities are below 10 mm per 5 min period. If $C_{soil,i}$ exceeds its maximum storage capacity ($S_{soil,i}$), infiltration does not occur and the water goes to the pipe network, if possible:

$$C_{pipe} = C_{pipe,t-1} + \sum_{i=3}^{6} R_{pipe,i} \quad (22)$$

or if $C_{pipe} > S_{pipe}$, then it goes to above ground runoff ($R_{AG,veg}$):

$$R_{AG,veg} = (C_{pipe} - S_{pipe}). \quad (23)$$

The total above ground runoff, or flooding, is then

$$R_{AG} = R_{AG,veg} + R_{AG,imp}$$

If the impervious surface is dry, water by evaporation is removed proportionally from the surrounding pervious surfaces. If evaporation occurs and the state of ith surface (C_i) is dry, water is removed from $C_{soil,i}$ under pervious surfaces:

$$C_{soil,i} = C_{soil,i,t-1} + R_{I,i} - E_i - R_{BG,i2j} - R_{DS} \quad (24)$$

where $R_{BG,i2j}$ is water flux between different soil storages and R_{DS} water flow to deep soil. If $C_{soil,i}$ is empty, no evaporation can occur.

After the vertical movement of water between the soil and atmosphere, water is allowed to move horizontally between the soil storages according to Green and Ampt's equation (Hillel, 1971); the water flux between soil stores i and j ($R_{BG,i2j}$):

$$R_{BG,i2j} = -K_{m,i2j}\frac{\Delta H_{i2j}}{X_{i2j}}, \quad (25)$$

where X_{i2j} is the distance between the two stores. The area of each surface type is assumed to be square and X_{i2j} is calculated as the distance between the midpoints. ΔH_{i2j} is the pressure head difference of the stores i and j and $K_{m,i2j}$ is the hydraulic conductivity. The pressure head (H_i) of each soil store (i) is calculated using van Genuchten (1980) with the assumption in their Eq. (3) of $m = 1$ and $n = 2$:

$$H_i = \frac{\sqrt{\Theta_i^{-2} - 1}}{\alpha_{vG}}, \quad (26)$$

where α_{vG} is a parameter ($\alpha_{vG} = 0.0005\ mm^{-1}$) and $\Theta_i = (\theta_{v,i} - \theta_{vr,i})/(\theta_{vs,i} - \theta_{vr,i})$ with the volumetric water content (θ_v) calculated from the soil moisture deficit:

$$\theta_v = \theta_{vs} - \frac{\Delta\theta}{z_{soil} f_r}$$

$K_{m,i2j}$ is calculated as an areally weighted average from the hydraulic conductivities of soils stores i and j (van Genuchten, 1980):

$$K_{m,i2j} = K_S \Theta_i^{0.5}[1 - (1 - \Theta_i^{n/(n-1)})^{1-1/n}]^2, \quad (27)$$

where K_s is the saturated hydraulic conductivity given as an input parameter and $n = 2$.

If at this point a below ground soil storage ($C_{soil,i}$) exceeds its maximum capacity ($S_{soil,i}$), the water is removed to deep soil as runoff (R_{DS}) given separately in the model output file. This is not

passed to the next grid cell. After these steps, the canopy and soil stores are updated and the model calculates the hourly evaporation, drainage, total runoff ($R = R_{pipe} + R_{AG}$) and runoff to deep soil (R_{DS}), soil moisture content and canopy state using the weighting of each surface fraction.

3. Methods

3.1. Measurements

SUEWS is tested against measured net-all wave radiation and turbulent fluxes of sensible and latent heat from Vancouver, Canada (Grimmond and Oke, 1991; Crawford et al., 2010) and from Los Angeles, USA (Grimmond and Oke, 1995). In addition, the modeled surface wetness and soil moisture are tested against measurements in Vancouver and the sensitivity to different model options in Vancouver in 1987 are shown.

The analysis undertaken here is for individual model grid areas (Fig. 1) rather than for a larger area. The sites used are located in Vancouver, Canada, and Los Angeles, USA (Table 4). The five datasets, referred to by site (SS) and year of measurements (YY) (combined to SSYY), are for Vancouver (Vo82, Vs87, Vo09, Vs09) and Los Angeles (Ar93, Ar94) (Table 4). For all datasets excluding Vo09 dynamically varying surface cover information were determined from turbulent source area analysis. For Vs09 the model by Korman and Meixner (2001) was used, while for Vs87, Ar93 and Ar94 the model of Schmid (1994) was used.

3.2. Parameter estimation

The parameter values for several of the functions used within the sub-models are obtained using a bootstrapping method (Efron and Gong, 1983) which allows more representative values and uncertainties to be assessed. In bootstrapping, the dataset is divided into 100 subsets, each with a random but arbitrary 5/6th of data, to allow measurement errors to be accounted for (Järvi et al., 2009). For each subset coefficients are determined. The final coefficients and root mean square errors (RMSE) are the arithmetic means and standard deviations of the 100 subsets.

The approach taken by function is:

(a) The *anthopogenic heat flux coefficients* for Eq. (3), are determined from multiple linear regression using the Vs87 data (Grimmond, 1992) (Table 4).
(b) The *surface resistance parameters* G_1–G_6 for Eq. (15) (Section 2.4.2) are calculated from non-linear least square regression between the 'measured' g_s (Eq. (16)) and the environmental variables ($K\downarrow$, T, Δq, $\Delta\theta$). Observations (Section 3.1) from five datasets (Vs87, Ar93, Ar94, Vs09, Vo09; Table 4) are used in order to generalize values for urban environments. The number of suitable datasets is limited as soil moisture is rarely measured together with the turbulent heat fluxes in urban areas.

The non-linear regression is conducted for daytime hours when the surface is dry. Daytime is defined by a positive $K\downarrow$ and the

Table 4
Characteristics of the measurement sites. For z_{0m}, z_d: Counihan (1971), Macdonald et al. (1998); RT: rule of thumb (Grimmond et al., 1999b). See Appendix A for other notation. Profiles see Table 3.

City	Vancouver				Los Angeles	
	Oakridge	Oakridge	Sunset	Sunset	Arcadia	Arcadia
Year	1982–1983	2009	1987	2009	1993	1994
Doy	22–22	178–243	33–179	1–365	186–223	188–205
Code	Vo82[a]	Vo09[b]	Vs87[c]	Vs09[b]	Ar93[d]	Ar94[e]
Location	49°23′N, 123°1′W	49°23′N, 123°1′W	49°23′N, 123°1′W	49°23′N, 123°1′W	34°08′N, 118°03′W	34°08′N, 118°03′W
A_s(ha)	21	22.5, 78[h]	21	78[h]	78.5	78.5
DLT_{Start}	73	67	67	67	94	94
DLT_{End}	331	305	305	305	304	304
f_{aut}	0.05	0.61	0.01	0.01	0.16	0.16
f_b	0.20	0.25[b]	0.26	0.23[a]	0.17	0.23
f_{con}	0.05	0.06	0.02	0.03	0.03	0.03
f_{dec}	0.14	0.19	0.07	0.09	0.31	0.28
$f_{Irrgrass}$	0.29	0.29	0.22	0.18	0.24	0.23
f_{pav}	0.20	0.20	0.27	0.45[a]	0.20	0.19
f_r	0.85	1	0.85	1	1	1
$f_{Unirrgrass}$	0.11	0.01	0.17	0.02	0.03	0.02
f_v	0.60	0.55	0.47	0.32[a]	0.61	0.56
f_w	0.01	0.00	0.00	0.00	0.02	0.02
I_e period	121–243	121–243	121–243	121–243	186–223	188–205
I_e profile	Prof2	8 pm–7 am 0.56	Prof1	Prof1	Prof2	Prof2
		7 am–4 pm 0.10				
		4 pm–8 pm 0.34				
p (in ha^{-1})	20.5	29.3	21.4	64.1[f]	18.7	18.7
T_{zone}	−9	−9	−9	−9	−8 (solar)	−8 (solar)
z_{0m}, z_d (m)	RT	RT	M	C	M	M
z_h (m)	7	5.8[g]	5.2	5.5[f]	5	5
z_{hv} (m)	7	8	6.0	7.1[f]	7	7
z_m (m)	9	29	22.5	28	30.5	32.5
z_{soil} (m)	–	0.05	0.15	0.05	0.08	0.08

[a] Grimmond and Oke (1986).
[b] Crawford et al. (2010).
[c] Grimmond and Oke (1991).
[d] Grimmond and Oke (1995).
[e] Grimmond et al. (1995).
[f] Average in long-term turbulent source area of tower.
[g] Determined for a representative segment of 10° and 500 m radius from the tower.
[h] Area studied a 500 m radius circle.

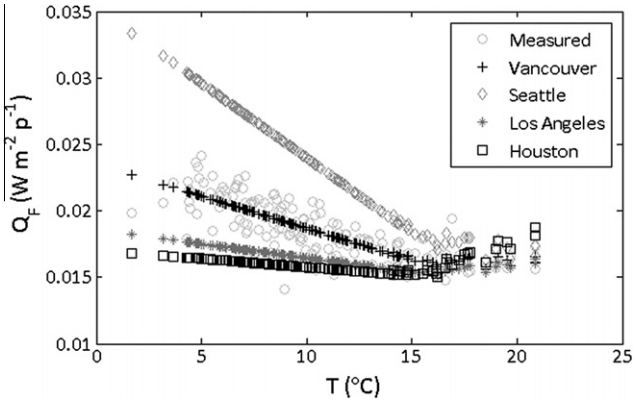

Fig. 2. 'Measured' (Grimmond, 1992) and modeled anthropogenic heat flux (Q_F) per capita^{-1} ha^{-1} as a function of air temperature T. The impact of coefficients from Seattle, Los Angeles and Houston are shown (Sailor and Vasireddy, 2006).

surface is assumed to be dry if rain had not been recorded in the preceding 3 h or the following 1 h. To fit the data, outliers defined as $g_s > 40$ mm s^{-1} (or $r_s < 25$ s m^{-1}), were omitted (see Fig. 3). Due to the different climatological and ecophysiological conditions, data were divided into seasons with winter extending from December to February (DJF), spring from March to May (MAM), summer from June to August (JJA) and fall from September to November (SON) (Table 5).

The coefficients were calculated by season and as a whole for Vancouver. For each season coefficients were determined based on a random 190 data points selected100 times through bootstrapping. The subsampled data were forced to have the similar numbers of samples per season and site: winter (DJF) 95 (Vs87) + 95 (Vs09), spring (MAM) 95 (Vs87) + 95 (Vs09), summer (JJA) 38 * 5 (All datasets), and fall (SON) 190 (Vs09) data points (Table 5a). The final coefficients for each season were calculated as an arithmetic mean from the 100 values (Table 5a). In addition, coefficients were determined 100 times for equally weighted seasonal amounts of data for Vancouver (190 * 3 + 38 * 3 = 684) and using 5/6th of the whole dataset (3509).

(c) For *external water use* (Section 2.3) coefficients for Eq. (5) are determined by multiple linear regression between the meteorological variables and water use data measured measured from 1 May–27 June in Vs87. The model is further tested with data collected between 28 April and 3 September in Vo82 and between 4 June and 23 September in Vs09. I_e data collected during Vs87 were also used to determine hourly water use profiles (Table 3). Water use profiles for the two sites in Los Angeles in Table 3 are from Grimmond et al. (1996).

4. Results of sub-model parameter development and testing

To evaluate model performance and to determine values for parameter coefficients, as many of the individual sub-models as possible are tested independently. The net all-wave radiation model has recently been evaluated in detail over a range of seasons (see Loridan et al., 2011). The performance of SUEWS is primarily

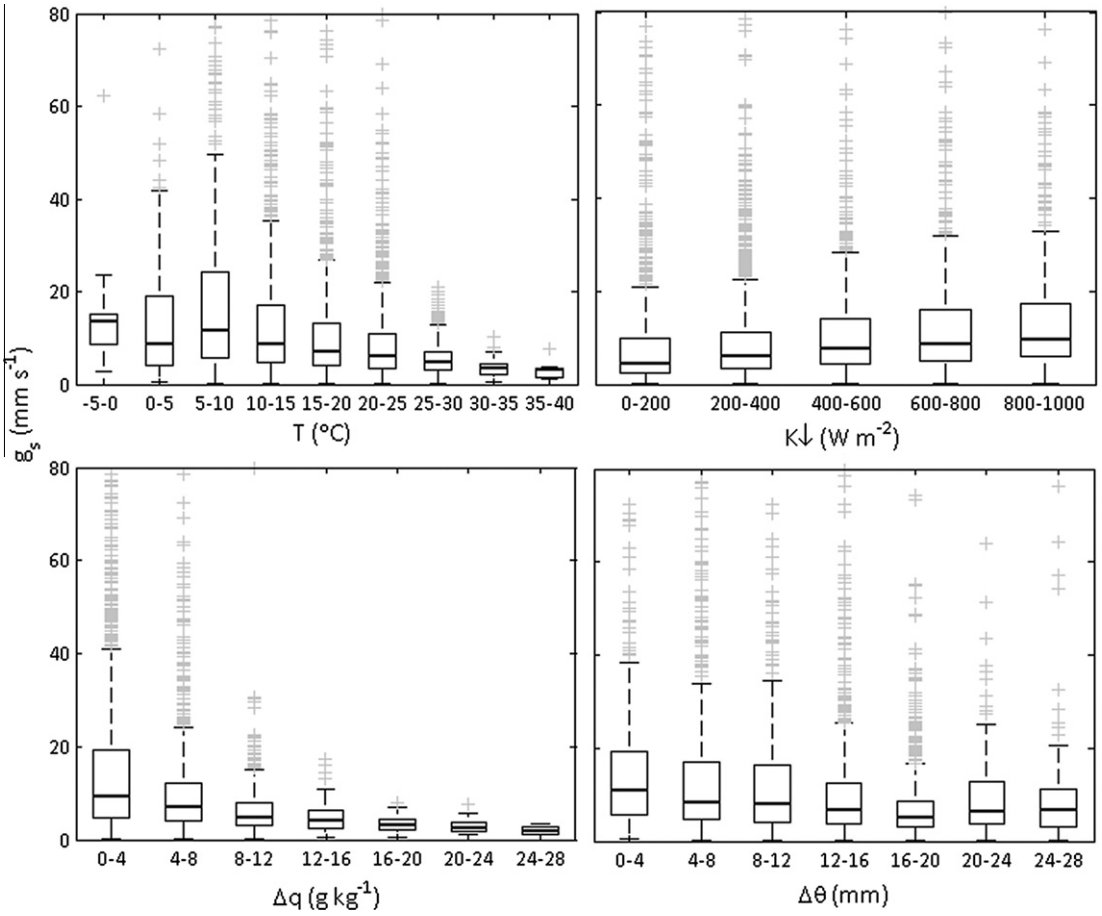

Fig. 3. Box plot of 'measured' surface conductance Eq. (16) with meteorological variables used in Eq. (15) to obtain the surface conductance parameters for the whole data set (see text for details). The outliers (+) (1.5 times the interquartile range) are show individually.

Table 5
Evaluation of g_s (a) total number of data points available by season for each dataset (see Table 4 for site codes) and (b) parameters values (G_1–G_6) calculated by seasons, cities and all data together. For the whole data set 25, 50 and 75th percentiles are shown, while for the others only medians are presented. *N* is the number of data points used in each bootstrapping run; winter (DJF), spring (MAM), summer (JJA), fall (SON). Bold: values used in the base run of the model.

Season	*Data set* (*number of hourly data points*)							
(a)	Vs09	Vo09	Vs87	Ar93	Ar94			
Winter	193	0	99	0	0			
Spring	606	0	647	0	0			
Summer	786	677	264	415	182			
Fall	342	0	0	0	0			
(b)	*N*	G_1 (mm s^{-1})	G_2 (W m^{-2})	G_3 (kg g^{-1})	G_4 (g kg^{-1})	G_5 (°C)	G_6 (mm)	RMSE (mm s^{-1})
Winter	190	5.68	26.0	0.148	8.91	9.43	0.007	8.92
Spring	190	14.97	1230.9	0.164	4.28	11.15	0.009	8.00
Summer	190	11.54	15906	0.093	8.27	19.56	0.013	5.39
Fall	190	7.87	131.1	0.132	5.95	17.88	0.040	7.27
Vancouver	684	14.97	359.1	0.213	3.32	9.42	0.016	8.73
50%	**760**	**16.48**	**566.1**	**0.216**	**3.36**	**11.07**	**0.018**	**8.53**
25%	760	13.80	435.0	0.191	3.24	11.53	0.018	8.37
75%	760	19.57	813.5	0.235	3.76	11.63	0.020	8.69
5/6th	3509	15.14	1462.3	0.180	4.17	13.50	0.015	7.16

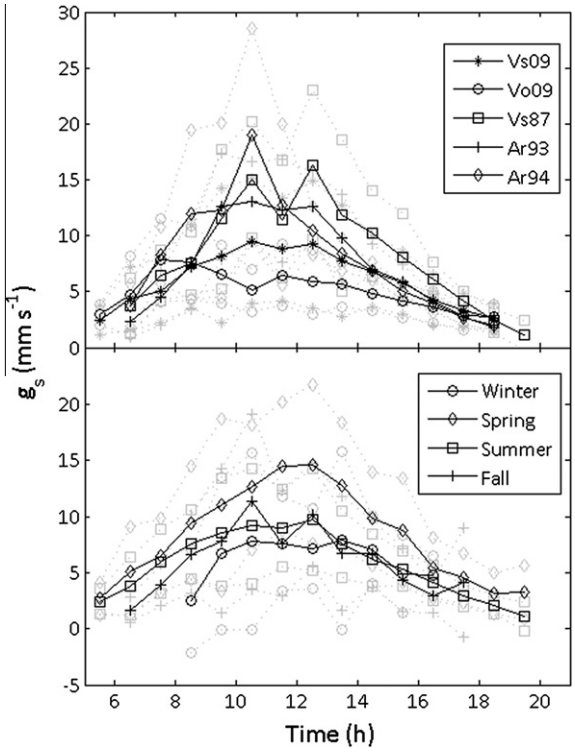

Fig. 4. Median diurnal behavior of 'measured' surface conductance g_s (mm s^{-1}) (a) for each dataset and (b) seasonally for all datasets together. The quartile deviations are shown with grey lines.

evaluated using the Vs87 dataset as this allows its performance to be considered relative to the original model (Grimmond and Oke, 1991) for which many more of the variables were required (and provided) as direct input. In addition, the Q^*, and turbulent fluxes are evaluated using four additional datasets Ar93, Ar94, Vs09 and Vo09. For each dataset the area modeled corresponds to the area calculated for the turbulent flux source area or for the catchment (Table 4).

4.1. Anthropogenic heat flux (Q_F)

Given the similarity in coefficients obtained (Eq. (3), Section 3.2) between weekdays and weekends, the same values are used here: $a_0 = (0.308 \pm 0.003)$ W m^{-2} (capita ha^{-1})$^{-1}$, $a_1 = (9.9 \pm 1.9) \cdot 10^{-3}$ W m^{-2} K^{-1} (capita ha^{-1})$^{-1}$, and $a_2 = (10.18 \pm 0.36) \cdot 10^{-3}$ W m^{-2} K^{-1} (capita ha^{-1})$^{-1}$ were obtained with RMSE = 0.028 W m^{-2}. Fig. 2 shows the Grimmond (1992) values relative to those modeled Q_F with Eq. (3) as a function of daily air temperature for Vs87. The temperature range for this data set is 1.5–21 °C; beyond this values should be used with caution.

The modeled flux gives the integrated Q_F for the study area and therefore it is strongly dependent on site characteristics and the behavior of the people in that area. The slope in response to cooling and heating degree days, for example, will vary depending on socio-cultural-economic factors of the city in question. Fig. 2 shows the shape of the functions for Seattle, Los Angeles and Houston (Sailor and Vasireddy, 2006) in comparison to Vs87. Heating need is small in Los Angeles and Houston and therefore there is little demand (slope $a_{2,\{wd,we\}}$) in cold temperatures, whereas the use of cooling is high and therefore $a_{1,\{wd,we\}}$ is larger. It should be noted that the slope values for Los Angeles, Houston and Seattle are based on city-scale analysis while the Vs87 results are determined at the neighborhood scale.

The Vs87 data are used to estimate the diurnal profile of Q_F separately for weekdays and weekends (Table 3). On workdays the effect of morning and evening rush hours on Q_F was evident. Otherwise the weekday and weekend daytime profiles were of the same order of magnitude indicating similar heat emissions from household activities and traffic in the study area.

4.2. Surface conductance (g_s)

The behavior of 'measured' g_s obtained from Eq. (16) with the meteorological variables T, $K\downarrow$, Δq and $\Delta\theta$ (Fig. 3) has the functional forms suggested by Jarvis (1976); this supports the use of this approach. Similarly, the diurnal behavior of the measured g_s at each site (Fig. 4a) follow those previously reported in the literature (Grimmond and Oke, 1991). The maximum conductances vary between 5 and 20 mm s^{-1}. Overall, the highest conductance values are observed in the Vs87 data set, not unexpectedly as they are spring time measurements and reflect conditions when leaves grow and take up carbon through stomata keeping the resistance to water exchange lower (Fig. 4b).

The results when 5/6th data points are used (Section 3.2) give coefficient values that are biased to the summer as there is much more data than for other seasons. To obtain a more general set of parameter values without this bias, the 190 data points from

seasonal datasets were used for the 100 bootstrapping runs. The final coefficients are the median values (50th percentile) from these 100 subsets (Table 5b). When measured and modeled g_s are compared using these parameters the RMSE is 7.4 mm s^{-1} (N = 15,168 h).

The parameters vary as a function of season with the weighting for the maximum surface conductance G_1 having its maximum in spring following the seasonal variations of g_s. The shortwave radiation related parameter G_2 has its highest value in summer when the solar radiation is most intense. The specific humidity deficit related parameters G_3 and G_4 peak in spring and winter, respectively. The temperature related G_5 reaches its maximum in fall, and the soil moisture related G_6 also reaches its maximum in fall when the soil is wettest. The fitted values for Los Angeles should be used with caution due to the small number of data points available for the analysis.

Fig. 5 shows the diurnal behavior of the functions $g(var)$ as calculated using the base values for all data sets together. $g(K\downarrow)$ follows the intensity of solar radiation on both the diurnal and annual scale and reaches the highest values in summer and lowest in winter. $g(\Delta q)$ reaches its maximum in early morning before reaching its minimum value defined by G_4. Thus in the daytime in summer, the humidity deficit is important in limiting Q_E. In winter, the importance of this function increases i.e. Q_E is less limited by humidity deficit. In summer, $g(T)$ decreases in the afternoon due to closure of stomata during the warmest hours of day. In winter the behavior is opposite and evaporation is enhanced during the warmest hours of day. $g(\Delta\theta)$ has flat diurnal course which is caused by the small diurnal variability of $\Delta\theta$. The correct biological/physical behavior of $g(var)$ suggests the fitted parameters are appropriate.

4.3. External water use (I_e)

The external water use (Section 2.3) coefficients for Eq. (5), when automatic irrigation was negligible (f_{aut} = 0.01, Vs87) are calculated (Section 3.2) to be $b_{0,a}$ = −84.54 ± 5.29 mm, $b_{1,a}$ = 9.96 ± 0.40 mm K^{-1} and $b_{2,a}$ = 3.67 ± 0.32 mm d^{-1} (RMSE = 1.14 mm d^{-1}). By comparing the median water use per property using manual irrigation and automatic sprinklers, calculated from Vo09 and Vs09, $b_{0,m}$–$b_{2,m}$ was found to be 0.30 times those from automatic irrigation. This gives R^2 = 0.80 and RMSE = 1.11 mm d^{-1} (with p-value 0.1) between the measured and modeled daily water use for Vs87.

The model was tested with water use measured during Vo82 and Vs09 (Fig. 6), where f_{aut} was estimated to be 0.05 and 0.01, respectively. The modeled water use follows the measured values well in Vo82 (R^2 = 0.73, RMSE = 3.57 mm d^{-1}) but has a larger RMSE for Vs09 where underestimation occurs (R^2 = 0.41, RMSE = 2.549 mm d^{-1}) particularly evident at times of higher water use (with a significance level of 0.9). If the hourly water use profile in Vs09 is assumed to follow that in 1987 (Table 3, Prof1), the R^2 = 0.36 and RMSE = 0.26 mm h^{-1}.

5. Results of application of SUEWS

5.1. Base run for Vs87

To evaluate the performance of the overall model a 'base' run is made using the Vs87 data (Table 4). Parameter values used for this run are listed in Tables 2 and 4. Initially, the soil stores are assumed to be full in winter as this is the wet period in Vancouver (Grimmond and Oke, 1986); surface stores were assumed to be dry. From roofs, 4% of water was allowed to flow on other surfaces, with the rest going directly to piped runoff (estimated rather than calibrated).

First, the individual energy balance fluxes (Q^*, Q_H and Q_E) are evaluated (Fig. 7, Table 6) at the hourly time scale for the whole measurement period. Not unexpectedly Q^* has the highest coefficient of determination (Table 6). This indicates the model gives good estimates of Q^* when downward longwave radiation is calculated using only T and RH (Loridan et al., 2011). This is important as errors in Q^* propagate into the turbulent fluxes. In Section 5.2 the effect of the modeled Q^* on latent heat flux is studied in more detail.

One of the intended improvements of SUEWS, compared to the Grimmond and Oke (1991) model, is the reduction in the number of variables that need to be supplied to use the model. Many of those required by Grimmond and Oke (1991) are not routinely

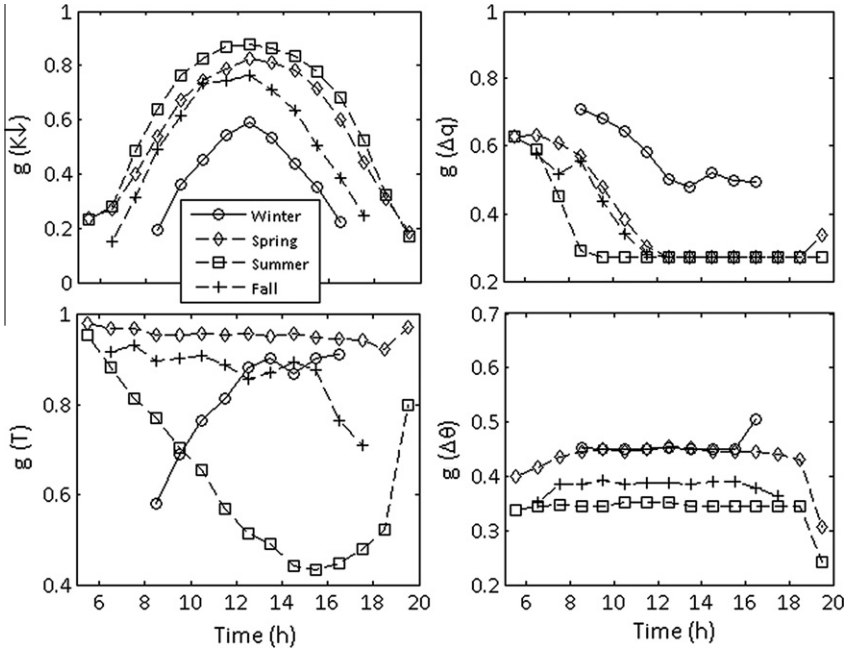

Fig. 5. Daytime median diurnal variation of functions g(var) in Eq. (15) by season calculated with the base run parameters G_1–G_6 for all data sets.

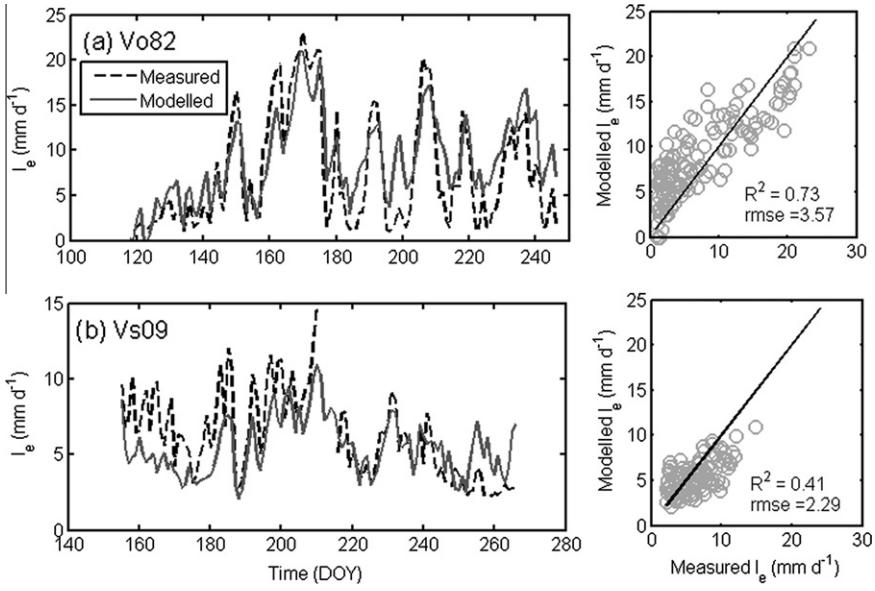

Fig. 6. Measured and modeled external water use I_e (mm d^{-1}) for Vo82 and Vs09 for the 21 and 22.5 ha area monitored, respectively.

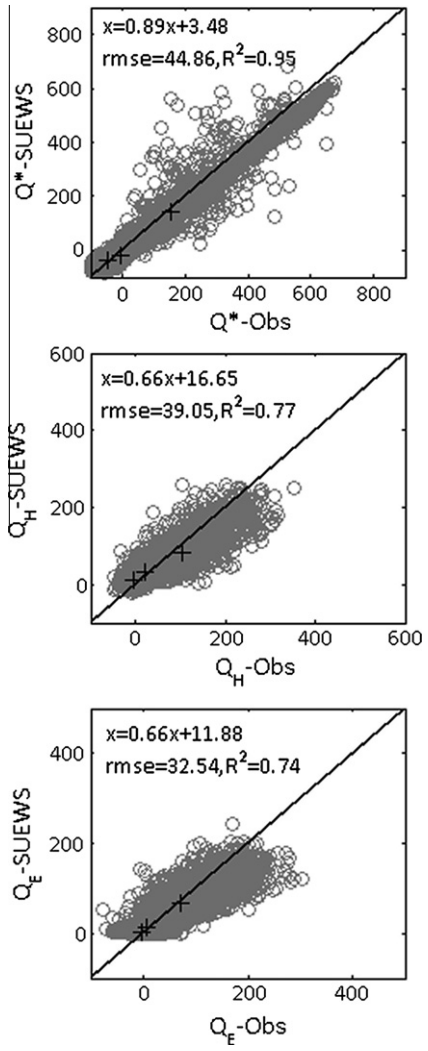

Fig. 7. Measured and modeled hourly net all-wave radiation Q^* and turbulent heat fluxes Q_H and Q_E for Vs87. The black pluses show the 25, 50 and 75 percentiles.

Table 6
Base run performance for hourly results for SUEWS and Grimmond and Oke (1991) [GO91 in table] for Vs87 data. NA indicates that the GO91 did not have this capability to model the so it is not applicable. See also Table 7 for more detailed analysis of SUEWS performance for Q_E.

Period:	Mean observed	SUEWS base		G091 Base	
22–179	W m^2	R^2	RMSE	R^2	RMSE
Q^*	75.9	0.95	44.9	NA	
Q_H	61.3	0.77	39.1	NA	
Q_E	38.8	0.74	32.5	0.81	27.7

measured. Statistics for the modeling of Q_E are slightly poorer than obtained by Grimmond and Oke (1991) (Table 6). However, given that previously the model was provided with observed Q^*, Q_H (for stability calculations), Q_F, I_e and $\Delta\theta$, this drop is regarded as acceptable (and expected) given these much reduced data inputs.

SUEWS underestimates Q_E in the daytime when the fluxes are larger resulting in a slight overestimation of Q_H (Fig. 8). When Q_E is low a slight overestimation of the flux occurs particularly in May and June. The model fails to simulate dew formation during the summer months. Currently the model does not account for snow accumulation and melt (beyond shortwave radiative exchanges).

Fig. 9 shows the time series of modeled irrigation and measured precipitation, surface wetness state of unirrigated lawn (plotted for between 0.05 and 1: wet) and $\Delta\theta$. The modeled surface state of unirrigated grass C_{UGR} and soil moisture deficit for the complete surface area weighted by plan area fraction for each component ($\Delta\theta$) and for each sub-surface i are also shown. The model simulates the surface wetness state well: only for 7% of the hours does the model predict a wet surface when the measured surface is dry, and in only 1% of the hours when the measured surface is wet does the model predict a dry surface. Thus overall, the model is able to follow the changes in the soil moisture following evaporation and precipitation events. The differences between the measured and modeled $\Delta\theta$ arise from the difficulty of measuring representative soil moisture relative to the volume the model is calculating for. Soil moisture measurements were carried out only below lawns, therefore they are not representative for the whole surface. At the hourly time scale, the different parts of the model respond

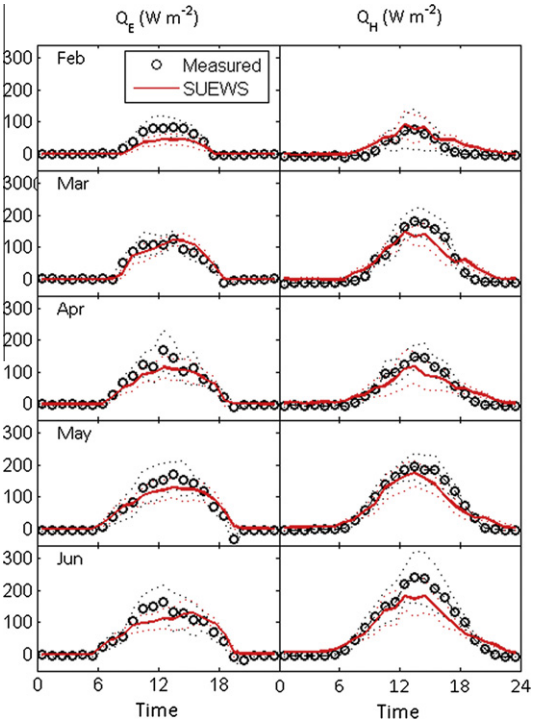

Fig. 8. Mean diurnal measured and modeled turbulent fluxes of (a) latent (Q_E) and b) sensible (Q_H) heat for Vs87. Dotted lines are quartile distributions.

appropriately to the precipitation and irrigation events indicating that the model can also be used to study short-term hydrological events.

At the monthly time scale, the model produces the expected temporal variability in the water balance results (Fig. 10). In winter, runoff dominates the water balance accounting for 85% of the water output in March. But, as the growing season starts, evapotranspiration becomes increasingly important reaching 91% of output in June when runoff is only 9%. In June, irrigation becomes the most important source (40%) for water with the remainder of the evaporative water coming equally from precipitation and soil drying. These results again are reasonable and show how the model is able to respond to the seasonal variations of the urban water balance and in future could be used for long-term water balance studies.

The maximum fluxes for the monthly energy balance are in June for Q^* with 128.6 W m^{-2} (11.1 MJ m^{-2} d^{-1}) and in February for Q_F 9.1 W m^{-2} (0.79 MJ m^{-2} d^{-1}) (Fig. 10). In February–March the turbulent fluxes are nearly the same, while in April–June more energy is partitioned into Q_H than to Q_E. In June Q_H reaches 71.4 W m^{-2} (6.17 MJ m^{-2} d^{-1}) and Q_E 49.6 W m^{-2} (4.29 MJ m^{-2} d^{-1}). These values compare well with the observations (Grimmond, 1992) (Fig. 10).

5.2. Sensitivity analysis of the model

To investigate the impact on Q_E sensitivity tests were run to assess the impact of model options (summarized in Table 7).

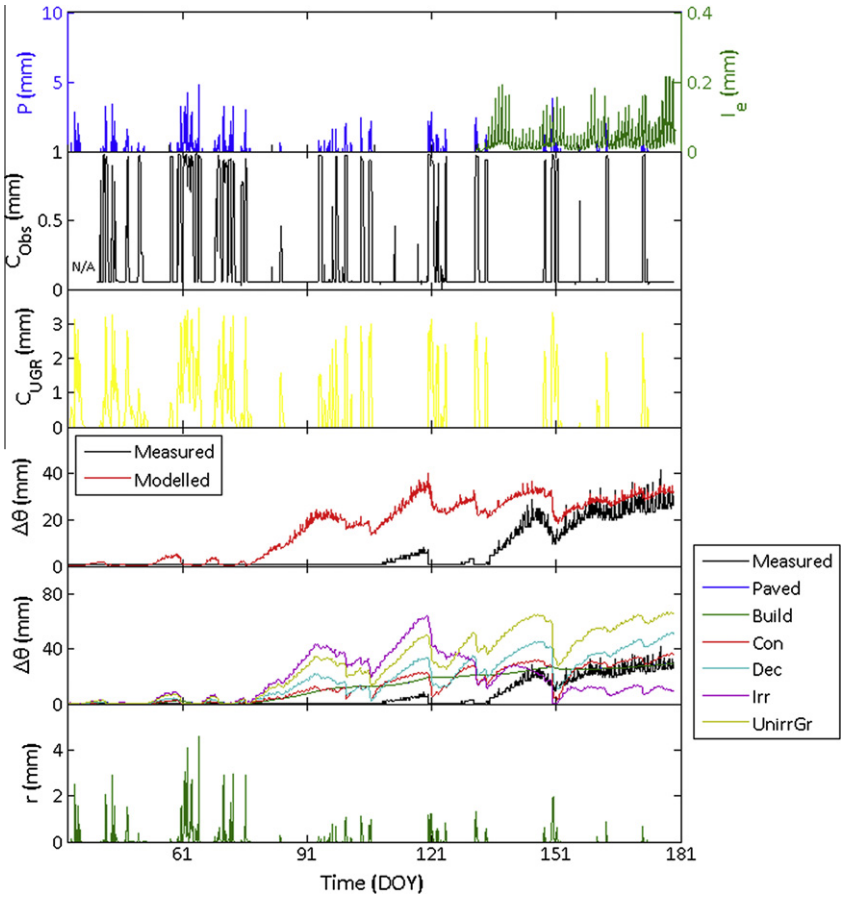

Fig. 9. Time series of hourly precipitation (p), modeled external water use (I_e), measured surface wetness state of unirrigated lawn, modeled surface state of unirrigated grass (C_{UGR}), net soil moisture deficit ($\Delta\theta$), soil moisture deficit of each sub-surface ($\Delta\theta_i$) and total runoff (R) in Vs87.

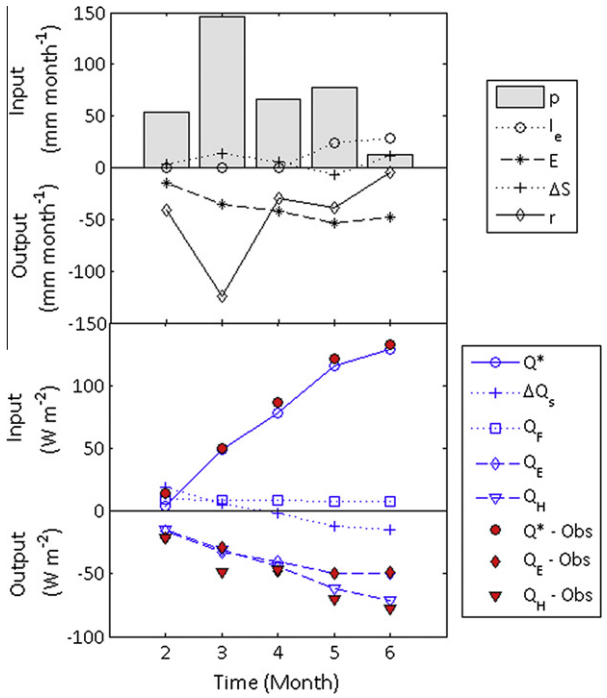

Fig. 10. Modeled monthly water (in mm month^{-1}) and energy balance fluxes (in W m^{-2}) in Vs87 for the period February (month 2) to June (month 6). Observed net all wave radiation, sensible and latent heat fluxes (Grimmond, 1992) are shown as solid points.

(a) *Net all wave radiation*: When measured Q^* is used, rather than modeled, there is only a minor improvement in modeled Q_E (R^2 of Q_E stays the same, RMSE decreases by 0.1 W m^{-2}). This is explained by the good agreement between the measured and modeled Q^* (Fig. 7a, Table 6).

(b) *Roughness length for heat*: The original $0.1z_{0m}$ gives slightly poorer model performance than the base run. Although, the z_{0m} exp(−20) proposed by Voogt and Grimmond (2000) improves the model performance, the parameterization given by Eqs. (13) and (14) are recommended as it allows varying vegetation cover to be accounted for. This term is important in energy balance models but uncertainty suggests there is need for ongoing research (Best et al., 2006; Loridan et al., 2010).

(c) *Surface conductance*: The effect of the surface conductance parameters (G_1–G_6) on the model performance is tested using 25th and 75th percentiles of the whole dataset and by using coefficients obtained for the different seasons (Table 4). The winter and fall values and 75th percentiles of the whole dataset give the poorest performance, with $R^2 < 0.69$ and RMSE > 36 mm s^{-1}, and strongly underestimate Q_E. Both spring and summer values give better model performance than the base run which uses parameter values obtained for whole year using all datasets. These values also decrease the underestimation of Q_E. Vs87 dataset contains measurements only from spring and early summer and it is likely therefore that better performance is obtained with these values. The 25th percentiles values do not have a large effect on the model performance.
These results show that these parameter values have a strong influence on how efficiently water is exchanged between the vegetation and atmosphere. Their importance is likely to decrease in areas with higher impervious surfaces due to the lack of vegetation.

(d) *Soil moisture deficit*: Using measured soil moisture deficit increases scatter between the modeled and measured Q_E (RMSE increases 2.4 W m^{-2}) but a better linear relation results (better R^2 and slope). The poorer model performance when using measured soil moisture likely indicate problems of spatial sampling and representativeness (Section 5.1).

(e) *External irrigation*: Using measured external water use has only a minor effect on the model performance indicating that the simple model provides a reasonable replacement to the observed values. A slightly larger effect on model performance was observed when the starting and ending days for the external irrigation were changed by 10 days. Specifying an earlier starting time of irrigation resulted in better model performance than the base run while the later one underestimates Q_E causing poorer performance.

These tests show the model to be most sensitive to the surface conductance parameters, while using the measured variables instead of the modeled ones had a minor impact on the model outputs.

5.3. Model performance at other measurement sites

In addition, the performance of the model is evaluated using datasets that Grimmond and Oke (1991) did not have to test their model. The newer datasets are used in the surface conductance model parameter calculations (Table 4). Evaluation is done on a seasonal basis (Fig. 11) with the Vs87 data included for comparison. The RMSE for Q^* varied from 25 (Vs09) to 47 W m^{-2} (Vs87), while for Q_H the range was from 30 (Vs87) to 64 W m^{-2} (Vo09), and for Q_E from 20 (Vs09) to 56 W m^{-2} (Ar93). In order to compare the performance between different seasons and fluxes, RMSE normalized with observed means were also calculated. For all three variables, the poorest model performance is observed in winter, particularly in Q^*. The model underestimates Q^* up to 50% and 20% through the day in Vs87 and Vs09, respectively (not shown). Also Q^* is underestimated slightly in fall. During other periods Q^* is modeled well but in Vancouver a slight nocturnal overestimation (maximum 50 W m^{-2} in Vs09 in fall) and in daytime a slight underestimation (maximum 50 W m^{-2} in Vs87 in summer) is observed, and in Los Angeles, Q^* is overestimated throughout the day by about 45 W m^{-2}.

During almost all seasons and sites excluding Vo09, Q_E is underestimated with highest underestimation 45 W m^{-2} observed in Vs09. SUEWS is able to model Q_E equally well in spring and summer with poorer performances in Los Angeles than in Vancouver. As Q_H is calculated as a residual, the underestimation of Q_E in most cases causes an overestimation of Q_H. In Vo09 both turbulent fluxes are overestimated indicating problems in Q_F and/or ΔQ_S.

SUEWS is able to model the net all-wave radiation and turbulent fluxes well and the RMSE vary in line with those reported in a recent urban land surface model comparison (Grimmond et al., 2011). When the RMSE of Q_E is normalized with the observed mean, the results for the sites (0.9–1.6) are at the better end of the model performances reported in Grimmond et al. (2011) (roughly 1.0–2.4). The best model performance was obtained for Q^* while the poorest for Q_H (not shown). This is the same overall conclusion as reported by Grimmond et al. (2011). As Q_H is the residual, errors from the other energy balance components accumulate. Q^* was modeled equally well in different seasons, whereas the turbulent fluxes are modeled better in summer.

The model responded as expected relative to fraction of impervious surface; with higher evaporation from sites with higher vegetation cover and lower runoff values modeled. At other sites, as for Vs87, the model responded as expected to precipitation and irrigation events. Modeled $\Delta\theta$ for the whole area was compared

Table 7
Statistics for sensitivity tests to options and variables in the calculation of Q_E (see text for details). All correlations are significant with p-value < 0.01. Observed and modeled distributions (25, 50 and 75th percentiles) are given.

	RMSE (W m^{-2})	R^2	Linear fit		Q_E (W m^{-2})		
			Slope	Intercept (W m^{-2})	25th percentile	Median	75th percentile
(a) Measured	–	–			−2.4	7.2	70.5
Base Run	**32.5**	**0.74**	0.68	11.4	**1.2**	**15.1**	**62.3**
(b) Measured *net all wave radiation*	32.4	0.74	0.70	11.1	0.6	12.2	67.9
(c) Roughness length for heat							
$0.1z_{0m}$	32.7	0.74	0.68	11.6	1.2	16.5	62.5
Voogt and Grimmond (2000)	29.1	0.79	0.77	8.5	1.0	7.9	58.9
(d) Measured *surface conductance*							
G_1–G_6: 25%	33.0	0.73	0.70	11.3	1.0	10.6	66.7
G_1–G_6: 75%	36.0	0.69	0.60	11.9	1.0	10.8	64.3
G_1–G_6: Winter (DJF)	46.8	0.47	0.43	14.5	1.0	9.8	59.0
G_1–G_6: Spring (MAM)	30.7	0.76	0.75	10.7	1.0	10.5	69.5
G_1–G_6: Summer (JJA)	31.3	0.76	0.75	7.8	1.0	8.9	55.9
G_1–G_6: Fall (SON)	37.2	0.67	0.59	12.1	1.0	10.4	64.1
(e) *Measured soil moisture deficit*	34.9	0.76	0.94	12.3	1.0	10.9	85.2
(f) *External Irrigation*							
Measured I_e	32.3	0.74	0.69	11.5	1.0	10.9	68.5
$I_{e,start}$, $I_{e,end}$ − 10 d	31.4	0.75	0.73	11.4	1.1	10.9	70.8
$I_{e,start}$, $I_{e,end}$ + 10 d	33.9	0.72	0.65	11.2	0.9	10.6	64.8

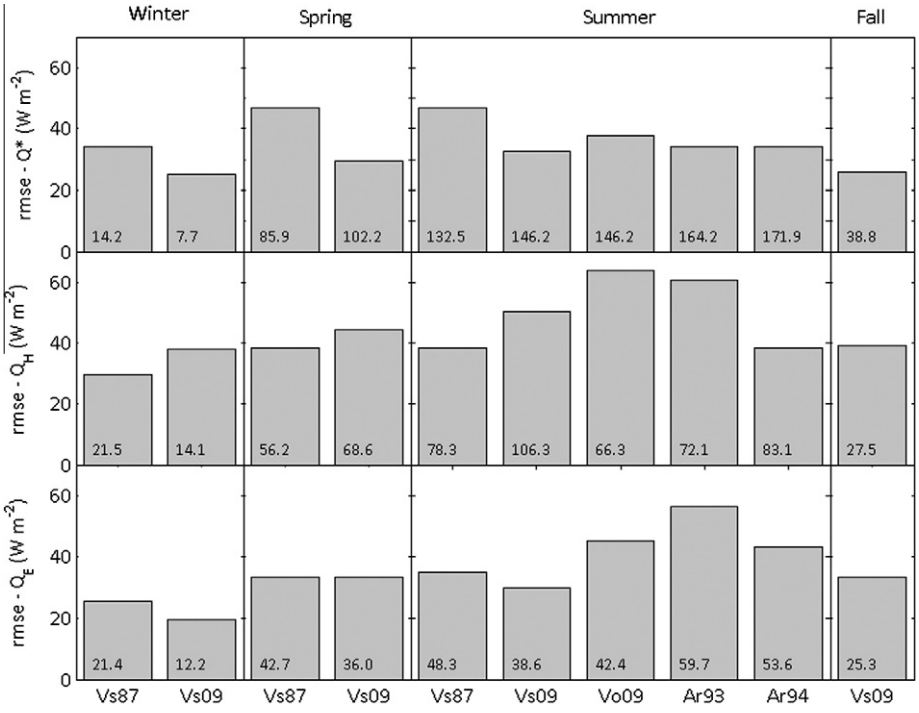

Fig. 11. Model performance (RMSE) for Q^*, Q_H and Q_E (W m^{-2}, bars) for five data sets by season. The mean observed values (W m^{-2}) are given at the bottom of each bar.

to $\Delta\theta$ measured under lawns in Vs09 and Vo09. Again SUEWS is able to model the variations in $\Delta\theta$ well at both sites, but predicts higher deficits than those measured (not shown). The differences originate from the different soil depth of the measurements and the model.

6. Conclusions

SUEWS is an urban energy and water balance model which requires only commonly measured meteorological forcing data and information about land cover (surface fractions) at the neighborhood scale. In the model the surface and soil have single-layer moisture stores with parallel stores for the different cover types. The model uses an hourly time step for the energy balance while it adopts 5-min time step for the water balance. In the model, the surface resistance scheme is parameterized explicitly for urban areas rather than using schemes originally designed for non-urban areas, and takes an integrated approach to the inclusion of urban vegetation.

The model is evaluated in Vancouver, Canada, and Los Angeles, USA, with five independent datasets. SUEWS is able to simulate the net all-wave radiation and turbulent fluxes of sensible and latent heat well, with RMSE varying between 25 and 47 W m^{-2}, 30 and 64 W m^{-2} and 20 and 56 W m^{-2}, respectively. The model also

tracks observed surface wetness state and soil moisture deficit well. It responds correctly to short-term events and to seasonal variations of the vegetation. The model is fairly insensitive to the model options which are introduced to limit the need for difficult to obtain forcing data. The largest uncertainty is related to the roughness length of heat and surface resistance.

Due to the simplicity of the model, SUEWS is easily usable; and has potential in evaluating planning decisions related to water conservation or restrictions, considerations of the mix of urban surface cover (e.g. increased or decreased vegetation), and for evaluating climate mitigation strategies where implications for heat and water need to be considered. The modeled sensible heat fluxes can be also used as forcing data (preprocessor) for dispersion modeling in air quality studies.

Acknowledgements

This work was supported by the Maj and Tor Nessling Foundation, Finnish Academy project (No:138328), European Commission under the EUf7 Grant Agreement No: 211345 (BRIDGE) and Canadian Foundation for Climate and Atmospheric Sciences (CFCAS) Environmental Prediction in Canadian Cities (EPiCC) network project. We would like to thank all those involved in the collection and analysis of the Vancouver and Los Angeles data sets; particularly, Nicholas Coops, Ben Crawford, Nicholas Goodwin, Rick Ketler, Kate Liss, Tim Oke, Rory Tooke and James Voogt.

Appendix A

Notation and input variables/parameters (marked with X) of the model in alphabetical order. For default values of input parameters see Tables 2 and 4 – those in **bold** are the most critical to be specific for a site. Parameters with subscript *i* in square brackets indicate they are used commonly and separately for the different surface types (*i*).

Variable	Units	Input	Table	Description
α_i	–	X	2	Effective surface albedo of *i*th sub-surface
α_{snow}	–	X	2	Effective surface albedo for snow
α_{vG}	mm^{-1}			Parameter in (26)
β	–			Bowen ratio
γ	hPa K^{-1}			Psychometric constant
$\Delta\theta$	mm			Soil moisture deficit
Δq	g kg^{-1}			Specific humidity deficit
ΔH_{i2j}	mm			Pressure head difference of stores *i* and *j*
ΔQ_S	W m^{-2}			Net storage heat exchange
ΔS	mm h^{-1}			Total water storage change
ε_i	–	X	2	Effective bulk surface emissivity of *i*th subsurface
ε_{snow}	–	X	2	Effective surface emissivity for snow
ζ	–			Atmospheric stability
$\theta_{v,[i]}$	m^3 m^{-3}			Volumetric water content
$\theta_{vr,[i]}$	m^3 m^{-3}			Residual volumetric water content of *i*th soil store
$\theta_{vs,[i]}$	m^3 m^{-3}			Saturated volumetric water content of *i*th soil store
υ	m^2 s^{-1}			Molecular viscosity of air
ρ	kg m^{-3}			Density of air
ρ_{soil}	kg m^{-3}			Soil density (needed if measured soil water content used)
ψ_m	–			Stability function for momentum
ψ_v	–			Stability function for heat and water vapor
Θ_i	–			Normalized volumetric water content of soil store *i*
a	–			Empirical parameter depending on surface cover (14)
$a_{0,\{wd,we\}}$	W m^{-2} (capita^{-1} ha^{-1})$^{-1}$	X	2	Parameter defining the base Q_F per capita in (3)
$a_{1,\{wd,we\}}$	W m^{-2} K^{-1} (capita^{-1} ha^{-1})$^{-1}$	X	2	Parameter related to CDD in (3)
$a_{2,\{wd,we\}}$	W m^{-2} K^{-1} (capita^{-1} ha^{-1})$^{-1}$	X	2	Parameter related to HDD in (3)
$\boldsymbol{A_s}$	**m^2**	**X**	**4**	**Surface area of the study grid**
b	–	X	2	Empirical coefficient in (18) and (19)
$b_{0,a}$–$b_{2,a}$	mm, mm K^{-1}, mm d^{-1}	X	2	Fitted parameters for automatic irrigation in (5)
$b_{0,m}$–$b_{2,m}$	mm, mm K^{-1}, mm d^{-1}	X	2	Fitted parameters for manual irrigation in (5)
c_p	J kg^{-1} K^{-1}			Specific heat capacity
$\boldsymbol{C_i}$	**mm**	**X**	**2**	**Interception state of the canopy of *i*th sub surface**
$C_{i,t-1}$	mm			Interception state of the canopy of *i*th sub surface from the previous time step
C_{pipe}	mm			Water storage state of pipe network
$C_{pipe,t-1}$	mm			Water storage state of pipe network from previous time step
$C_{soil,i}$	**mm**	**X**	**2**	**Wetness state of the soil**
$C_{soil,I,t-1}$	mm	X	2	Wetness state of the soil from the previous time step
CDD	°C			Cooling degree days

(*continued on next page*)

Appendix A (*continued*)

Variable	Units	Input	Table	Description
doy	–			Day of year
$D_{[i]}$	mm h^{-1}			Drainage
$D_{0,i}$	mm	X	2	Drainage rate when $C_i \geqslant S_i$
$D_{S2S,[i]}$	mm			Part of drainage flowing to other sub-surfaces
$\boldsymbol{DLT_{Start}}$	**doy**	**X**	**4**	**Start of the daylight savings time (used for I_e and Q_F)**
$\mathbf{DLT_{End}}$	**doy**	**X**	**4**	**End of the daylight savings time (used for I_e and Q_F)**
$E_{[i]}$	mm h^{-1}			Evaporation
$\boldsymbol{f_{aut}}$	**–**	**X**	**4**	**Fraction of irrigated surface area using automatic irrigation**
$\boldsymbol{f_b}$	**–**	**X**	**4**	**Plan area fraction of roofs**
$\boldsymbol{f_{con}}$	**–**	**X**	**4**	**Plan area fraction of coniferous trees**
$\boldsymbol{f_{dec}}$	**–**	**X**	**4**	**Plan area fraction of deciduous trees**
$\boldsymbol{f_i}$	–			Plan area fraction of surface type *i*
$\boldsymbol{f_{Irrgrass}}$	**–**	**X**	**4**	**Plan are fraction of irrigated grass**
$\boldsymbol{f_{pav}}$	**–**	**X**	**4**	**Plan area fraction of paved surfaces**
$\boldsymbol{f_r}$	**–**	**X**	**4**	**Fraction of soil without rocks**
$f_{Unirrgrass}$	–	**X**	**4**	**Plan are fraction of unirrigated grass**
$\boldsymbol{f_v}$	**–**	**X**	**4**	**Plan area fraction of vegetation**
$\boldsymbol{f_w}$	**–**	**X**	**4**	**Plan area fraction of water**
F	mm h^{-1}			Anthropogenic water emission
g_s	m s^{-1}			Surface conductance
$g_{i,max}$	m s^{-1}			Maximum conductance values of vegetation type *i*
$g(var)$	–			Surface conductance functions in (15)
G_1	mm s^{-1}	X	2	Parameter related to the maximum surface conductance in (15)
G_2	W m^{-2}	X	2	Parameter in $g(K\downarrow)$
G_3	kg g^{-1}	X	2	Parameter in $g(\delta q)$
G_4	g kg^{-1}	X	2	Parameter in $g(\delta q)$
G_5	°C	X	2	Parameter in $g(T)$
G_6	mm	X	2	Parameter in $g(\delta\theta)$
$GDD_{[i]}$	°C	X	2	Growing degree days when leaf-on
H_i	mm			Pressure head of soil store *i*
HDD	°C			Heating degree days
i	–			Surface cover type
$I_{[e]}$	mm h^{-1}			External piped water supply
$\boldsymbol{I_{e,start}}$	**doy**	**X**	**4**	**Starting day for external irrigation**
$\boldsymbol{I_{e,end}}$	**doy**	**X**	**4**	**Ending day for external irrigation**
$\boldsymbol{I_{WB}}$	**mm**	**X**	**2**	**Additional water supplied to the water surface type (see text)**
j	–			Soil store, surface store
k	–			von Karman constant
K	–			Related r_a and r_s in (7)
$\boldsymbol{K\downarrow}$	**W m^{-2}**	**X**	**1**	**Incoming shortwave radiation**
$K\downarrow_m$	W m^{-2}	X	2	Maximum incoming shortwave radiation used in $g(K\downarrow)$
$K\uparrow$	W m^{-2}			Outgoing shortwave radiation
$K_{m,i2j}$	mm s^{-1}			Hydraulic conductivity of soil storage *i*
K_s	mm s^{-1}	X	2	Saturated hydraulic conductivity of soil
lat	**–**	**X**	**4**	**Latitude of the site**
lon	**–**	**X**	**4**	**Longitude of the site**
L	m			Obukhov length
$L\downarrow$	W m^{-2}			Incoming longwave radiation
$L\uparrow$	W m^{-2}			Outgoing longwave radiation
$L_{m,i}$	m^2 m^{-2}			Maximum *LAI* of vegetation type i
L_v	J kg^{-1}			Latent heat of vaporization
LAI	m^2 m^{-2}			Leaf area index
$LAI_{d,i}$	m^2 m^{-2}			Daily leaf area index of vegetation type i
$LAI_{Max,i}$	m^2 m^{-2}	X	2	Maximum annual *LAI* of vegetation type *i*
$LAI_{Min,i}$	m^2 m^{-2}	X	2	Minimum annual *LAI* of vegetation type *i*
LUCY	–			Large scale Urban Consumption of energy model
LUMPS	–			Local scale urban parameterization scheme
n	–			Parameter in (27)
N	–			Number of data points
NARP	–			Net all-wave radiation parameterization scheme
OHM	–			Objective Hysteresis Model

Appendix A (*continued*)

Variable	Units	Input	Table	Description
p	**capita ha^{-1}**	**X**	**4**	**Population density inside the grid**
P	**mm h^{-1}**	**X**	**1**	**Precipitation**
Q^*	W m^{-2}			Net all-wave radiation
Q_E	W m^{-2}			Latent heat flux
Q_F	W m^{-2}			Anthropogenic heat emission
$Q_{F,p\{wd,we\}}$	W m^{-2} K^{-1} (capita^{-1} ha^{-1})$^{-1}$			Anthropogenic heat emission per capita separated to weekdays and weekends
Q_H	W m^{-2}			Sensible heat flux
r_a	s m^{-1}			Aerodynamic resistance
r_b	s m^{-1}			Mean boundary layer resistance
r_s	s m^{-1}			Surface resistance
$r_{s,max}$	s m^{-1}			Maximum surface resistance
r_{ss}	s m^{-1}			Redefined surface resistance
res_{cap}	mm	X	2	Capacity of the surface to hold water (LUMPS)
res_{drain}	mm h^{-1}	X	2	Drainage rate of water bucket (LUMPS)
R	mm h^{-1}			Total runoff
R_{AG}	mm			Above ground runoff
$R_{AG,imp}$	mm			Above ground runoff from impervious surfaces
$R_{AG,veg}$	mm			Above ground runoff from pervious surfaces
$R_{BG,i2j}$	mm			Horizontal transfer of water between surface types i and j
R_C	mm	X	2	Limit of surface is totally covered with water (LUMPS)
$R_{I[,i]}$	mm			Infiltration into subsurface i
$R_{G2G,[i]}$	mm			Water obtained from other grids via above ground runoff
$R_{Pipe,[i]}$	mm			Runoff to pipe network
$R_{S2S,[i]}$	mm			Water flowing from other sub-surfaces
$R_{DS,[i]}$	mm			Runoff to deep soil
RH	**%**	**X**		**Relative humidity**
s	hPa K^{-1}			Slope of the saturation vapor pressure curve
S_1	mm	X	2	Fitted parameter related to maximum $\Delta\theta$ in (15)
S_2	mm	X	2	Fitted parameter related to maximum $\Delta\theta$ in (15)
S_i	mm	X	2	Maximum storage capacity of ith surface
S_{Pipe}	mm	X	2	Maximum depth capacity of pipes
$\boldsymbol{S_{soil,i}}$	**mm**	**X**	**2**	**Maximum storage capacity of *i*th soil store**
$SDD_{[i]}$	°C	X	2	Senescence degree days
t	**h**	**X**	**1**	**Time**
$\boldsymbol{t_r}$	d			Days since rain
T	**°C**	**X**	**1**	**Air temperature**
$T_{BaseGDD}$	°C	X	2	Base temperature for vegetation growth of ith vegetation surface
$T_{BaseSDD}$	°C	X	2	Base senescence temperature of ith vegetation surface
T_{BaseQF}	°C	X	2	Base temperature for Q_F
T_d	°C			Daily mean air temperature
T_H	°C	X	2	Maximum air temperature limit in (17)
T_L	°C	X	2	Minimum air temperature limit in (17)
$\boldsymbol{T_{step}}$	**s**	**X**	**2**	**Time step**
$\boldsymbol{T_{zone}}$	**h**	**X**	**4**	**Time zone relative to UTC**
u	**m s^{-1}**	**X**	**1**	**Horizontal wind speed**
u^*	m s^{-1}			Friction velocity
V	hPa			Vapor pressure deficit of air
wd	–			Weekdays
we	–			Weekends
W	–			Function of C_i relative to S_i
X	–			Stability dependence of the unstable stability function for momentum
X_{i2j}	m			Distance between two soil stores
Y	–			Stability dependence of the unstable stability function for heat and water vapor
z_{0m}	m			Roughness length for momentum
z_{0v}	m			Roughness length for heat and water vapor
z_d	m			Zero displacement height
$\boldsymbol{z_h}$	**m**	**X**	**4**	**Mean building height**
$\boldsymbol{z_{hv}}$	**m**	**X**	**4**	**Mean vegetation height**
$\boldsymbol{z_m}$	**m**	**X**	**4**	**Height of the wind speed measurements**
z_{soil}	m	X	4	Depth of the soil layer

References

Allen, L., Lindberg, F., Grimmond, C.S.B., 2010. Global to city scale model for anthropogenic heat flux: model and variability. Int. J. Clim. doi:10.1002/joc.2210.

Aston, A., 1977. Water resources and consumption in Hong Kong. Urban Ecol., 2327–2353.

Bell, F.C., 1972. The acquisition, consumption and elimination of water by Sydney urban system. Proc. Ecol. Soc. Aust. 7, 160–176.

Berthier, E., Andrieu, H., Creutin, J.D., 2004. The role of soil in the generation of urban runoff: development and evaluation of a 2D model. J. Hydrol. 299, 252–266.

Berthier, E., Dupont, S., Mestayer, P.G., Andrieu, H., 2006. Comparison of two evaporation schemes on a sub-urban site. J. Hydrol. 328, 635–646.

Best, M.J., Grimmond, C.S.B., Villani, M.G., 2006. Evaluation of the urban tile in MOSES using surface energy balance observations. Boundary-Layer Meteorol. 118, 503–525.

Breuer, L., Eckhardt, K., Frede, H.-G., 2003. Plant parameter values for models in temperate climates. Ecol. Model. 169, 237–293.

Brutsaert, W., 1982. Evaporation into the Atmosphere: Theory, History, and Applications. Kluwer Academic Publishers, Netherlands.

Campbell, T., 1982. La Ciudad de Mexico como ecosistema. Ciencias Urbanas 1, 28–35.

Counihan, J., 1971. Wind tunnel determination of the roughness length as a function of fetch and density of three-dimensional roughness elements. Atmos. Environ. 5, 637–642.

Crawford, B., Christen, A., Ketler, R., 2010. EPiCC Technical Report 1: Processing and Quality Control Procedures of Turbulent Flux Measurements During the Vancouver EPiCC Experiment. <http://www.geog.ubc.ca/≃epicc/reports/Vancouver-EPiCC-Tech-Report-1.pdf>.

Cuo, L., Lettenmaier, D.P., Mattheussen, B.V., Storck, P., Wiley, M., 2008. Hydrologic prediction for urban watersheds with the Distributed Hydrology-Soil-Vegetation Model. Hydrol. Process 22, 4205–4213.

Davies, H., Hollis, T., 1981. Measurements of rainfall-runoff volume relationships and water balance for roofs and roads. Second International Conference on Urban Storm Drainage, Urbana, Illinois.

Efron, B., Gong, G., 1983. A leisurely look at the bootstrap the jackknife, and cross validation. Am. Stat. 37, 36–48.

Falk, J., Niemczynowicz, J., 1978. Characteristics of the above ground runoff in sewered catchments. In: Helliwell, P.R. (Ed.), Urban Storm Drainage. Pentech, London.

Gober, P., Kirkwood, C.W., Balling, R.C., Ellis, A.W., Deitrick, S., 2010. Water planning under climatic uncertainty in Phoenix: why we need a new paradigm. Ann. Assoc. Am. Geogr. 100, 356–372.

Grimmond, C.S.B. 1988. An Evaporation Interception Model for Urban Areas. Ph.D. thesis, University of British Columbia, Vancouver.

Grimmond, C.S.B., 1992. The suburban energy balance: methodological considerations and results for a mid-latitude west coast city under winter and spring conditions. Int. J. Clim. 12, 481–497.

Grimmond, C.S.B., Oke, T.R., 1986. Urban water balance 2: results from a suburb of Vancouver, British Columbia. Water Resour. Res. 22, 1404–1412.

Grimmond, C.S.B., Oke, T.R., 1991. An evaporation-interception model for urban areas. Water Resour. Res. 27, 1739–1755.

Grimmond, C.S.B., Oke, T.R., 1995. Comparison of heat fluxes from summertime observations in the suburbs of four North American cities. J. Appl. Meteor. 34, 873–889.

Grimmond, C.S.B., Oke, T.R., 1999a. Heat storage in urban areas: observations and evaluation of a simple model. J. Appl. Meteorol. 38, 922–940.

Grimmond, C.S.B., Oke, T.R., 1999b. Aerodynamic properties of urban areas derived from analysis of surface form. J. Appl. Meteorol. 38, 1262–1292.

Grimmond, C.S.B., Oke, T.R., 2002. Turbulent Heat Fluxes in Urban Areas: Observations and a Local-Scale Urban Meteorological Parameterization Scheme (LUMPS). J. Appl. Meteorol. 41, 792–810.

Grimmond, C.S.B., Best, M., Barlow, J., Arnfield, A.J., Baik, J.-J., Belcher, S., Bruse, M., Calmet, I., Chen, F., Clark, P., Dandou, A., Erell, E., Fortuniak, K., Hamdi, R., Kanda, M., Kawai, T., Kondo, H., Krayenhoff, S., Lee, S.H., Limor, S.-B., Martilli, A., Masson, V., Miao, S., Mills, G., Moriwaki, R., Oleson, K., Porson, A., Sievers, U., Tombrou, M., Voogt, J., Williamson, T., 2009. Urban surface energy balance models: model characteristics & methodology for a comparison study. In: Baklanov, A., Grimmond, C.S.B., Mahura, A. (Eds.), Urbanization of Meteorological & Air Quality Models. Springer-Verlag, Athanassiadou, pp. 97–123.

Grimmond, C.S.B., Blackett, M., Best, M., Barlow, J., Baik, J.J., Belcher, S., Bohnenstengel, S.I., Calmet, I., Chen, F., Dandou, A., Fortuniak, K., Gouvea, M.L., Hamdi, R., Hendry, M., Kawai, T., Kawamoto, Y., Kondo, H., Krayenhoff, E.S., Lee, S.H., Loridan, T., Martilli, A., Masson, V., Miao, S., Oleson, K., Pigeon, G., Porson, A., Ryu, Y.H., Salamanca, F., Steeneveld, G.J., Tombrou, M., Voogt, J., Young, D., Zhang, N., 2010. The international urban energy balance models comparison project: first results from Phase 1. J. Appl. Meteorol. Clim. 49, 1268–1292. doi:10.1175/2010JAMC2354.1.

Grimmond, C.S.B., Blackett, M., Best, M.J., Baik, J.-J., Belcher, S.E., Beringer, J., Bohnenstengel, S.I., Calmet, I., Chen, F., Coutts, A., Dandou, A., Fortuniak, K., Gouvea, M.L., Hamdi, R., Hendry, M., Kanda, M., Kawai, T., Kawamoto, Y., Kondo, H., Krayenhoff, E.S., Lee, S.-H., Loridan, T., Martilli, A., Masson, V., Miao, S., Oleson, K., Ooka, R., Pigeon, G., Porson, A., Ryu, Y.-H., Salamanca, F., Steeneveld, G.J., Tombrou, M., Voogt, J.A., Young, D.T., Zhang, N., 2011. Initial results from Phase 2 of the international urban energy balance model comparison. Int. J. Clim. 31, 244–272. doi:10.1002/joc.2227.

Grimmond, C.S.B., Oke, T.R., Steyn, D.G., 1986. Urban water balance 1. A model for daily totals. Water Resour. Res. 22, 1397–1403.

Grimmond, C.S.B., Souch, C., Hubble, M.D., 1996. Influence of tree cover on summertime surface energy balance fluxes, San Gabriel Valley, Los Angeles. Clim. Res. 6, 45–57.

Halldin, S., Grip, H., Perttu, K., 1979. Model for energy exchange of a pine forest canopy. In: Halldin, S. (Ed.), Comparison of Forest Water and Energy Exchange Models. International Society of Ecological Modeling.

Hillel, D., 1971. Soil and Water: Physical Principles and Processes. Academic Press, New York.

Högström, U., 1988. Non-dimensional wind and temperature profiles in the atmospheric surface layer: a re-evaluation. Boundary-Layer Meteorol. 42, 55–78.

Irmak, S., Mutiibwa, D., 2010. On the dynamics of canopy resistance: generalized linear estimation and relationships with primary micrometeorological variables. Water Resour. Res. 46, W08526. doi:10.1029/2009WR008484.

Jarvis, P.G., 1976. The interpretation of the variations in leaf water potential and stomatal conductance found in canopies in the field. Philos. Trans. R. Soc. London, Ser. B. 273, 593–610.

Järvi, L., Hannuniemi, H., Hussein, T., Junninen, H., Aalto, P.P., Hillamo, R., Mäkelä, T., Keronen, P., Siivola, E., Vesala, T., Kulmala, M., 2009. The urban measurement station SMEAR III: continuous monitoring of air pollution and surface-atmosphere interactions in Helsinki, Finland. Boreal Environ. Res. 14 (Suppl. A), 86–109.

Kanda, M., Kanega, M., Kawai, T., Moriwaki, R., Sugawara, H., 2007. Roughness lengths for momentum and heat derived from outdoor urban scale models. J. Appl. Meteorol. Clim. 46, 1067–1079.

Kawai, T., Ridwan, M.K., Kanda, M., 2009. Evaluation of the simple urban energy balance model using selected data from 1-yr flux observations at two cities. J. Appl. Meteorol. Clim. 48, 693–715.

Korman, R., Meixner, F.X., 2001. An analytical footprint model for non-neutral stratification. Boundary-Layer Meteorol. 99, 207–224.

L'vovich, M.I., Chernogayeva, G.M., 1977. Transformation of water-balance within city of Moscow. Sov. Geogr. 18, 302–312.

Lemonsu, A., Masson, V., Berthier, E., 2007. Improvement of the hydrological component of an urban soil-vegetation-atmosphere-transfer model. Hydrol. Processes 21, 2100–2111.

Lindh, G., 1978. Urban hydrological modelling and catchment research in Sweden. In: McPherson, B. (Ed.), Research on Urban Hydrology, vol. 2. UNESCO, Paris, pp. 229–265.

Loridan, T., Grimmond, C.S.B., Crossman-Clarke, S., Chen, F., Tewari, M., Manning, K., Martilli, A., Kusaka, H., Best, M., 2010. Trade-offs and responsiveness of the single-layer urban canopy parametrization in WRF: An offline evaluation using the MOSCEM optimization algorithm and field observations. Q. J. Roy. Meteor. Soc. 136, 997–1019.

Loridan, T., Grimmond, C.S.B., Offerle, B.D., Young, D.T., Smith, T., Järvi, L., Lindberg, F., 2011. Local-scale urban meteorological parameterization scheme (LUMPS): longwave radiation parameterization and seasonality-related developments. J. Appl. Meteor. Climatol. 50, 185–202.

Macdonald, R.W., Griffiths, R.F., Hall, D.J., 1998. An improved method for estimation of surface roughness of obstacle arrays. Atmos. Environ. 32, 1857–1864.

MacDonald, D.H., Crossman, N.D., Mahmoudi, P., Taylor, L.O., Summers, D.M., Boxall, P.C., 2010. The value of public and private green spaces under water restrictions. Landscape Urban Plan. 95, 192–200.

McMichael, A.J., Wilkinson, P., Kovats, R.S., Pattenden, S., Hajat, S., Armstrong, B., Vajanapoom, N., Niciu, E.M., Mahomed, H., Kingkeow, C., Kosnik, M., O'Neill, M.S., Romieu, I., Ramirez-Aguilar, M., Barreto, M.L., Gouveia, N., Nikiforov, B., 2008. International study of temperature, heat and urban mortality: the 'ISOTHUM' project. Int. J. Epidemiol. 37, 1121–1131.

Mitchell, V.G., Mein, R.G., McMahon, T.A., 2001. Modelling the urban water cycle. Environ. Modell. Softw. 16, 615–629.

Mitchell, V.G., McMahon, T.A., Mein, R.G., 2003. Components of the total water balance of an urban catchment. Environ. Manage. 32, 735–746.

Mitchell, V.G., Cleugh, H.A., Grimmond, C.S.B., Xu, J., 2008. Linking urban water balance and energy balance models to analyze urban design options. Hydrol. Process 22, 2891–2900.

Monteith, J.L., 1965. Evaporation and environment. Symp. Soc. Exp. Biol. 19, 205–224.

Offerle, B., Grimmond, C.S.B., Oke, T.R., 2003. Parameterization of Net All-Wave Radiation for Urban Areas. J. Appl. Meteorol. 42, 1157–1173.

Offerle, B., Grimmond, C.S.B., Fortuniak, K., 2005. Heat storage and anthropogenic heat flux in relation to the energy balance of a central European city centre. Int. J. Clim. 25, 1405–1419.

Oke, T.R., 1987. Boundary Layer Climates. Routledge, London, UK.

Penman, H.L., 1948. Natural evaporation from open water, bare soil and grass. Proc. R. Soc. London, Ser. A. 193, 120–145.

Roberts, S.M., Oke, T.R., Grimmond, C.S.B., Voogt, J.A., 2006. Comparison of four methods to estimate urban heat storage. J. Appl. Meteorol. Clim. 45, 1766–1781.

Rutter, A.J., Kershaw, P.C., Robins, P.C., Morton, A.J., 1971. A predictive model of rainfall interception in forests, 1, Derivation of the model from observations in a plantation of Corsician pine. Agric. Meteorol. 9, 367–384.

Sailor, D.J., Vasireddy, C., 2006. Correcting aggregate energy consumption data account for variability in local weather. Environ. Modell. Softw. 21, 733–738.

Schiff, K., Bax, B., Markle, P., Fleming, T., Newman, J., 2007. Wet and dry weather toxicity in the San Gabriel River. Bulletin, Southern California Academy of Sciences 106, 179–192.

Schmid, H.P., 1994. Source area for scalars and scalar fluxes. Boundary Layer Meteorology 67, 293–318.

Shuttleworth, W.J., 1978. A simplified one-dimensional theoretical description of the vegetation-atmosphere interaction. Boundary-Layer Meteorol. 14, 3–27.

Shuttleworth, W.J., 1983. In: Street-Perrott, A., Beran, M., Radeliffe, R.D. (Eds.), Variations in the Global Water Budget: Evaporation Models in the Global Water Budget. Reidel, Hingham, Mass.

van Genuchten, M.Th., 1980. A closed-form equation for predicting the hydraulic conductivity of unsaturated soils. Soil Sci. Soc. Am. J. 44, 892–898.

van Ulden, A.P., Holtslag, A.A.M., 1985. Estimation of atmospheric boundary layer parameters for boundary layer applications. J. Clim. Appl. Meteorol. 24, 1196–1207.

Voogt, J.A., Grimmond, C.S.B., 2000. Modeling surface sensible heat flux using surface radiative temperatures in a simple urban area. J. Appl. Meteorol. 39, 1679–1699.

Xiao, Q., McPherson, E.G., Simpson, J.R., Ustin, S.L., 2007. Hydrological processes at the urban residential scale. Hydrol. Process. 21, 2174–2188.